Geophysical Journal International

Geophys. J. Int. (2011) **187,** 1301–1318 doi: 10.1111/j.1365-246X.2011.05223.x

Seismic, petrological and geodynamical constraints on thermal and compositional structure of the upper mantle: global thermochemical models

Fabio Cammarano,[1]★ Paul Tackley[2] and Lapo Boschi[2]

[1]*Department of Geology and Geography, University of Copenhagen, Øster Voldgade 10, 1350, Copenhagen, Denmark. E-mail: fc@geo.ku.dk*
[2]*Institute of Geophysics, ETH Zürich, Sonneggstrasse 5, 8091, Switzerland*

Accepted 2011 September 5. Received 2011 September 5; in original form 2011 January 17

SUMMARY

Mapping the thermal and compositional structure of the upper mantle requires a combined interpretation of geophysical and petrological observations. Based on current knowledge of material properties, we interpret available global seismic models for temperature assuming end-member compositional structures. In particular, we test the effects of modelling a depleted lithosphere, which accounts for petrological constraints on continents. Differences between seismic models translate into large temperature and density variations, respectively, up to 400 K and 0.06 g cm^{-3} at 150 km depth. Introducing lateral compositional variations does not change significantly the thermal interpretation of seismic models, but gives a more realistic density structure. Modelling a petrological lithosphere gives cratonic temperatures at 150 km depth that are only 100 K hotter than those obtained assuming pyrolite, but density is ∼0.1 g cm^{-3} lower. We determined the geoid and topography associated with the density distributions by computing the instantaneous flow with an existing code of mantle convection, STAG-YY. Models with and without lateral variations in viscosity have been tested. We found that the differences between seismic models in the deeper part of the upper mantle significantly affect the global geoid, even at harmonic degree 2. The range of variance reduction for geoid due to differences in the transition zone structure (i.e. from 410 to 660 km) is comparable with the range due to differences in the whole mantle seismic structure. Since geoid is dominated by very long wavelengths (the lowest five harmonic degrees account for more than 90 per cent of the signal power), the lithospheric density contrasts do not strongly affect its overall pattern. Models that include a petrological lithosphere, however, fit the geoid and topography better. Most of the long-wavelength contribution that helps to improve the fit comes from the oceanic lithosphere. The signature of continental lithosphere worsens the fit, even in simulations that assume an extremely viscous lithosphere. Therefore, a less depleted, and thus less buoyant, continental lithosphere is required to explain gravity data. None of the seismic tomography models we analyse is able to reproduce accurately the thermal structure of the oceanic lithosphere. All of them show their lowest seismic velocities at ∼100 km depth beneath mid-oceanic ridges and have much higher velocities at shallower depths compared to what is predicted with standard cooling models. Despite the limited resolution of global seismic models, this seems to suggest the presence of an additional compositional complexity in the lithosphere.

Key words: Gravity anomalies and Earth structure; Composition of the mantle; Elasticity and anelasticity; Seismic tomography.

1 INTRODUCTION

The evolution of our planet is governed by its interior dynamics. To understand the nature of such dynamics, it is essential to determine the current temperature (T) and compositional (C) conditions, since these two fundamental parameters determine the physical properties (rheology, elasticity, etc.) of the Earth. A multidisciplinary approach, which includes geophysical and petrological observations and knowledge of material properties, is required to obtain a global picture of the Earth's mantle. With this in mind, we present here a family of thermochemical models that are inferred from the interpretation of seismic models for given compositional structures. We

★Formerly at: Institute of Geophysics, ETH Zürich, Sonneggstrasse 5, 8091, Switzerland.

test, in particular, the effects of including a petrological lithosphere, which is characterized by depleted compositions. All the thermochemical models are tested for their ability to fit geodynamical (geoid and topography) observations.

Samples of rocks or mineral fragments are carried to the Earth's surface from the uppermost mantle (down to ∼200 km depth) by processes related to mantle convection. Their mineralogy and geochemical signatures inform us about their origins (McDonough & Sun 1995; O'Neill & Palme 1998). For example, it is possible to retrieve pressure (P) and temperature at the time of their formation, and thus determine their original depth. Together with cosmochemical data (Palme & O'Neill 2003), petrological and geochemical studies allow us also to model the primitive mantle material from which they originated. However, a large part of the mantle is inaccessible to direct sampling and, therefore, most of our knowledge on its structure and physical conditions relies on the interpretation of geophysical measurements recorded at the Earth's surface. In particular, the analysis of seismic waves has been remarkably successful for investigating deep structure. The propagation of seismic waves through the Earth depends on its elastic and anelastic properties. Through experimental or theoretical studies of mantle material at appropriate P–T conditions, we can estimate the relationship between such physical properties and T and C.

The constantly growing quality and quantity of seismic data results in global models of increasingly high resolution (e.g. Panning & Romanowicz 2006; Boschi *et al.* 2007; Simmons *et al.* 2010). In spite of these advances, quantitative interpretations of the seismic models (and data) in terms of T and C have been hampered until very recently. Early attempts were based on the conversion of seismic anomalies to temperatures, assuming a given composition (Goes & van der Lee 2002). To decouple thermal and compositional effects, gravity and geoid data have also been used (e.g. Forte & Mitrovica 2001; Deschamps *et al.* 2007; Forte *et al.* 2010) because density varies strongly with composition, whereas temperature variations are dominant for velocity (e.g. Cammarano *et al.* 2003). Topography and plate-motion data have been included as well (e.g. Forte & Perry 2000; Perry *et al.* 2003).

Previous studies on the thermochemical structure of the upper mantle (Forte & Perry 2000; Deschamps *et al.* 2002; Perry *et al.* 2003) were able to provide first compositional maps (in terms of iron-depletion) of continental roots and to determine that chemical depletion of continents is less than what is measured in xenolith samples at surface.

A combined interpretation of seismic and gravity data (and possibly of other geophysical measurements) surely helps to better constrain the thermal and compositional structure of the upper mantle, but it is not clear to what extent classical linearized inversion schemes (see Simmons *et al.* 2010, for a nice example of joint inversion for lower mantle structure) can be used for this purpose. First, geoid kernels are computed based on the strong assumption of a 1-D viscosity profile. Second, the relation between seismic velocity and density introduces, inevitably, further uncertainties. The mineral physics relation which links those two parameters depends on uncertain elastic and, more importantly, anelastic parameters. Furthermore, parametrization and weighting of different data used also involves a great deal of subjective choices.

Here, we do not attempt a joint inversion of seismic and gravity data; rather, we assess how uncertainties in seismic structure and composition of the upper mantle affect geodynamic observations. Unlike previous studies, we rely on a self-consistent thermodynamic model to relate seismic velocities and density to temperature and composition (Xu *et al.* 2008) and we include physically based anelasticity corrections. We also discuss the role of mineral physics uncertainties assessed in previous work (Cammarano *et al.* 2003; Cammarano & Romanowicz 2008; Cobden *et al.* 2008, 2009).

Our analysis provides an insight on the current knowledge of the thermal and compositional conditions of the Earth's upper mantle. The main questions addressed are: what is the effect of a 'petrological lithosphere' on seismic and gravity interpretation? Are structural differences between seismic tomography models large enough to translate into quantitatively significant differences in temperature and density?

2 PROCEDURE

Our methodology consists of the following steps:

(1) Seismic velocities and density as a function of P, T and C are computed. We use thermodynamic modelling to identify the mineralogy and elastic properties of the aggregate, and we correct for viscoelastic relaxation (anelasticity) effects at seismic frequencies. The reference mineral physics model is the same as in the study of Cammarano *et al.* (2009).

(2) We assume various compositional structures and use the relationships established in step '1' to convert seismic tomography maps into distributions of density (ρ) and T. We model, in particular, the compositional variations within the lithosphere on the basis of petrological constraints. Four different seismic models are considered. The same crustal model (CRUST2.0, Bassin *et al.* 2000) is assumed for all the models. In addition, we also model the density structure of a (age-dependent) half-space cooling model of the oceanic lithosphere.

(3) We compute the instantaneous mantle flow, surface topography and geoid with a numerical fluid-dynamical code, STAG-YY (Tackley 2008). The code is in spherical geometry and is able to handle large variations in viscosity. Hence, we were able to test several viscosity structures, assessing the role of lateral variations in viscosity (LVV) as well.

(4) Synthetic geoid and topography maps are compared with observations. A spectral analysis of the results is performed.

(5) We compare the thermochemical structures with each other, assessing how their variations affect the fitting of geoid and topography observations.

The global thermochemical models are distributed through the Internet: jupiter.ethz.ch/∼fabioca/UM-TC-models.html. The 3-D models include temperature, composition, density, seismic velocities (V_P and V_S), attenuation (i.e. the inverse of quality factor, $1/Q_S$) and viscosity values.

Although we focus on the effect of upper-mantle structure on geoid and topography, we also provide whole mantle models in which the lower mantle structure is always the same, as described later. To reproduce sufficiently well the predicted mineralogical aspects of the models with depth, we parametrize the vertical direction quite finely (each 10 km), while horizontally we expand all fields in spherical harmonics up to degree 24. It should be noted that these features are not resolved by gravity and seismic observations used here, but predicted on the basis of our mineral physics model. Our models can be useful in a variety of contexts, from comparison with T–C resulting from geodynamic modelling, to modelling electrical conductivity and test its effect on the induced magnetic field (e.g. Kuvshinov & Olsen 2006).

3 DATA AND METHODS

3.1 Modelling the material properties of the upper mantle

3.1.1 Phase equilibria and elasticity

For a given chemical composition (C), the assemblage of minerals that are stable at high P–T can be determined experimentally (e.g. Ito & Takahashi 1989; Ohtani & Sakai 2008) or through thermodynamical modelling (Stixrude & Lithgow-Bertelloni 2005; Kuskov *et al.* 2006). Currently, phase equilibria and elastic properties of the mantle can be modelled within a rigorous thermodynamical framework for a 6-oxide system (NCFMAS system, i.e. sodium-calcium-iron-magnesium-aluminum and silicon) (Xu *et al.* 2008). This model, named XSLB08, and already used by Cammarano *et al.* (2009), is also implemented here. We use PerpleX (www.perplex.ethz.ch, Connolly 2005), a software for thermodynamical modelling that includes XSLB08, for computing the phase equilibria. Once the assemblage of minerals and their individual elastic properties are known at given P–T and C conditions, the properties for the bulk rock are estimated using the classical VHR (Voigt–Reuss–Hill) averaging scheme (Hill 1952).

3.1.2 Anelasticity

The importance of including anelasticity for interpreting seismic anomalies has long been recognized (Karato 1993; Cammarano *et al.* 2003). The strong T-dependence of anelasticity introduces a non-linearity in the relation between V_S and T. This effect is expected to be more pronounced in regions where T approaches the solidus, such as at the base of the lithosphere.

Anelastic properties are much more uncertain than elastic properties (Cammarano *et al.* 2009). The dominant attenuation mechanism at seismic frequencies is still under debate and no experimental data yet exist at elevated pressure. For this reason, we model anelasticty effects by using simple physical laws that are valid for bulk rock assemblages. Specifically, we model the P, T and frequency dependency of anelasticity by using the simple models of Cammarano *et al.* (2003). Namely, the quality factor Q_S, that is the inverse of seismic attenuation, is modelled as

$$Q_S = B\omega^a \exp\left(\frac{agT_S(P)}{T}\right) \tag{1}$$

with

$$g = \frac{H(P)}{RT_S(P)}, \tag{2}$$

where B is a normalization factor, ω seismic frequency, a the exponent describing the frequency dependence of the attenuation (fixed to 0.2 in all the models of Cammarano *et al.* 2003), P the pressure, R the gas constant, H the activation enthalpy and T_S is the solidus temperature. The dimensionless factor g is assumed to be constant with pressure (or depth). The P-dependence is modelled, this way, with what is known as a 'homologous-T approach' (Karato 1993): the attenuation is scaled at any depth with respect to the solidus temperature. We test the models of Cammarano *et al.* 2003, with $g = 30$ and $g = 15$, plus a model obtained assuming $g = 40$. The models span extreme values for the experimentally observed Arrhenian temperature dependence. The pre-exponential values (B) were adjusted on the basis of constraints from seismically observed attenuation at a reference frequency of 1 Hz, and assuming a reference thermal profile (i.e. a 1300° adiabat). As in Cammarano *et al.* (2009), we do not consider variations in Q_S due to composition, grain size or partial melt.

3.1.3 Viscosity

Since our main goal is to assess how the density distributions of our thermochemical models are able to fit geodynamic observations, we adopt the same viscosity structure for all models shown and discussed in the paper, that is, viscosity profile V1 by Mitrovica & Forte (2004), also implemented in Forte *et al.* (2010). This viscosity profile captures the main features of the current understanding of viscosity in the Earth's mantle. Specifically, the presence of a low-viscosity layer around 100–300 km and a sharp increase in viscosity (by a factor 30–100) in the mid-mantle (Richards & Hager 1984).

We also tested, however, T-dependent LVV. We only vary the viscosity structure within the upper mantle, while the V1 model is assumed as a fixed reference for the lower mantle. Our tests on the effects of T-dependent LVV are documented in supporting material (Figs S1–S5 in Supporting Information) and basically confirm previous findings: the effect of LVV is secondary to its variation with depth for fitting the geoid (e.g. Zhang & Christensen 1993; Moucha *et al.* 2007; Ghosh *et al.* 2010). In addition, we also tested the effect of highly viscous continental blocks, by increasing the viscosity of the continental lithosphere by three orders of magnitude compared to what is predicted by a purely P–T-dependent viscosity law.

Adding rigid tectonic plates and weak plate boundaries is essential to obtain the toroidal component of the flow (Zhang & Christensen 1993), and is also important for accurately modelling geoid and topography (Forte 2007). However, it is not the aim of this study to infer viscosity structure or the most appropriate boundary conditions. To compare the different thermochemical models between each other, it is sufficient to use a single boundary condition. We choose to run simulations using simple free-slip conditions.

3.2 Modelling the compositional structures

There are two sorts of compositional variations that we consider in this paper. The first type is related to the variation with depth of chemical composition. In our earlier studies on the average thermochemical structure of the upper mantle (Cammarano & Romanowicz 2007; Cammarano *et al.* 2009), we found that seismic data are consistent with a mixture of two chemical compositions, harzburgite and MORB, with C becoming more enriched in MORB with increasing depth (starting from ∼250 km). This C structure, as discussed in the mentioned papers, is dynamically feasible (Tackley *et al.* 2005) and may help to explain several geochemical observations. Such a 'mechanical mixture' (i.e. not chemically homogeneous), a term first introduced by Xu *et al.* 2008, could survive within the Earth because of the low chemical diffusivities of mantle minerals (Allègre & Turcotte 1986; Xu *et al.* 2008), but further evidence is needed to prove its existence. In this paper, we assume either the C2 profile of Cammarano *et al.* 2009 (here called MM-C2), that starts very depleted (10 per cent of MORB content at 200 km) and reaches ∼40 per cent of MORB at 660 km, or homogeneous pyrolite, as radially symmetric C structures.

The second type of compositional variations, more important, regards lateral heterogeneity. Lateral variations in composition (ΔC) within the lithosphere are modelled based on petrological constraints.

In this study, we are interested in modelling the main feature of compositional variations at lithospheric depths, that is, the

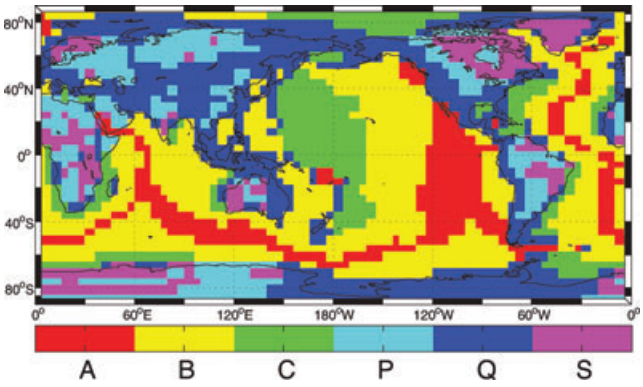

Figure 1. Global Tectonic Regionalization (GTR1) model (Jordan 1981). S, Q and P are, respectively, precambrian shield and platforms, phanerozoic orogenic zones and magmatic belts and phanerozoic platforms. A, B and C are young (0 to 25 Myr), intermediate (25 to 100 Myr) or old (>100 Myr) oceanic crust. The colour scheme is used for all regionalized T and ρ profiles shown afterward.

dichotomy in composition between the depleted (old) continental areas and the 'normal' mantle. We rely on a simple parametrization, which accounts for tectonic regionalization at the surface and varying thickness of the chemical boundary layer.

For continental areas, we use the GTR1 (global tectonic regionalization) model (Jordan 1981), illustrated in Fig. 1. This is a $5^\circ \times 5^\circ$ grid model mapping shield and platforms of exposed Archean and Proterozoic rocks (category S), platforms overlain by Phanerozoic cover (P) and Phanerozoic orogenic and magmatic belts (Q). At each of these three regions, we assign a single bulk chemical composition based on a global compilation of xenoliths and their related interpretation (Griffin *et al.* 2009, see Table 1). Additionally, we assume a depleted (harzburgite) C for the oceanic lithosphere (Table 1). The specific composition of pyrolite and mid-ocean ridge basalt (MORB) used is also given. We use the same self-consistent thermodynamic model (XSLB08) to compute the properties for all the compositions given in Table 1.

The thickness of the chemical lithosphere (sometimes called chemical boundary layer or CBL) is inferred from the thermal interpretation of the seismic model. It is expected that the rheological behaviour changes as T reaches ∼85 per cent of the melting T. The transition, that is often associated with a change in seismic anisotropy, can therefore be modelled with a temperature isosurface (or isotherm) of ∼1200 °C (but other isotherms have been tested as well). In principle, the CBL is not strictly related to the thermal boundary layer (TBL). Xenolith studies, however, indicate a similarity in thickness between the two, at least at long wavelengths (Griffin & Ryan 1995; Artemieva 2009). For oceanic regions, we also test the lithosphere thickness based on a simple relation with the age of oceanic crust: $h \simeq \sqrt{2\kappa t}$), where κ is the thermal diffusivity, taken as 10^{-6} m^2 s^{-1}, and t is time. The age of the oceanic crust is obtained from the model of Müller *et al.* (2008).

For our first-order petrological lithosphere, we do not model any compositional variation with depth within the continental lithosphere, contrary to what is observed in xenolith studies (e.g. by Griffin *et al.* 2009), and no lateral variations in composition are assumed below the lithosphere.

Table 1. Chemical compositions (mol per cent).

	Pyrolite[a]	MORB[a]	Harzburgite[a]	P[b]	Q[b]	S[b]
SiO_2	38.71	51.75	36.04	37.64	37.79	35.19
MgO	49.85	14.94	56.54	52.83	53.84	60.09
FeO	6.17	7.06	5.97	6.01	5.55	4.41
CaO	2.94	13.88	0.79	2.08	1.62	0.09
Al_2O_3	2.22	10.19	0.65	1.19	1.04	0.14
Na_2O	0.11	2.18	0.0	0.25	0.16	0.08

[a]These compositions are the same used in Xu *et al.* (see references therein).
[b]The bulk compositions for P, Q and S provinces of the GTR1 models are modelled by using petrology constraints on the subcontinental lithospheric mantle. We use, respectively, the compositions of the Tectons, Protons and Archons provinces of Griffin *et al.* 2009. The composition for the precambrian shield and platforms (S) is an average estimate of the pristine Archaean C that characterizes the top part of the lithosphere and the less depleted composition inferred from garnet systematics of mantle xenoliths. Original chemical compositions are simplified to have only the six NCFMAS components.

3.3 Seismic constraints

Long-period seismic data (down to a period of 60 s) provide the most comprehensive global constraint on upper-mantle shear velocity (V_S) structure. Fundamental-mode surface waves (Rayleigh and Love) are mostly sensitive to the uppermost mantle structure (down to ∼250–300 km) and the inclusion of overtones provides resolution in the transition zone (Cammarano & Romanowicz 2007). On the other hand, body wave traveltimes, P and S, have only a partial upper-mantle coverage. Therefore, models that use only body waves (e.g. Grand 2002; Montelli *et al.* 2006; Simmons *et al.* 2010) are not used in this study. Overall, the seismic structure of the Earth's mantle is well constrained by available tomography models at long wavelengths, but the correlation between the models degrades at shorter scale lengths (Becker & Boschi 2002).

In Fig. 2, we show slices at 150 km depth of four recent tomography V_S models (see caption), all expanded up to spherical harmonic degree (ℓ) 24 (corresponding to a horizontal resolution of ∼1000 km). The isotropic component (Voigt average) of these radially anisotropic models is shown. While radial anisotropy at the top of the upper mantle is essential to fit simultaneously Rayleigh and Love waves (e.g. Dziewonski & Anderson 1981), the seismic data used are primarily sensitive to isotropic V_S structure, which is therefore well constrained. At 150 km, correlation between the models is very high. We systematically find a correlation coefficient of ∼0.9 (Fig. S6, Supporting Information), while the correlation decreases to only ∼0.2 in the transition zone and increases again (up to ∼0.5) in the lower mantle. This typical pattern, already noted by Becker & Boschi (2002), holds also for the most recent V_S models and shows the difficulty in recovering the structure of the transition zone (e.g. Ritsema *et al.* 2004).

3.3.1 *Average seismic structure*

Because of the non-linearity in the relation between V_S and T introduced by anelasticity, it is necessary to use absolute values of seismic velocities to interpret the models correctly. Therefore, the choice of the seismic reference model is very important. Cammarano *et al.* (2003, 2005a,b); Cammarano & Romanowicz (2007); Cobden *et al.* (2009) and Cammarano *et al.* (2009) show that long-period waveforms are able to constrain absolute values of $<V_S>(z)$ in the upper mantle, but they cannot resolve sharp transitions. Yet, if sharp transitions are included in the starting model, they would affect the average of the final 3-D model, which is obtained by using perturbation theory (Cammarano & Romanowicz 2007; Styles *et al.* 2011). For purely seismological purposes, this does

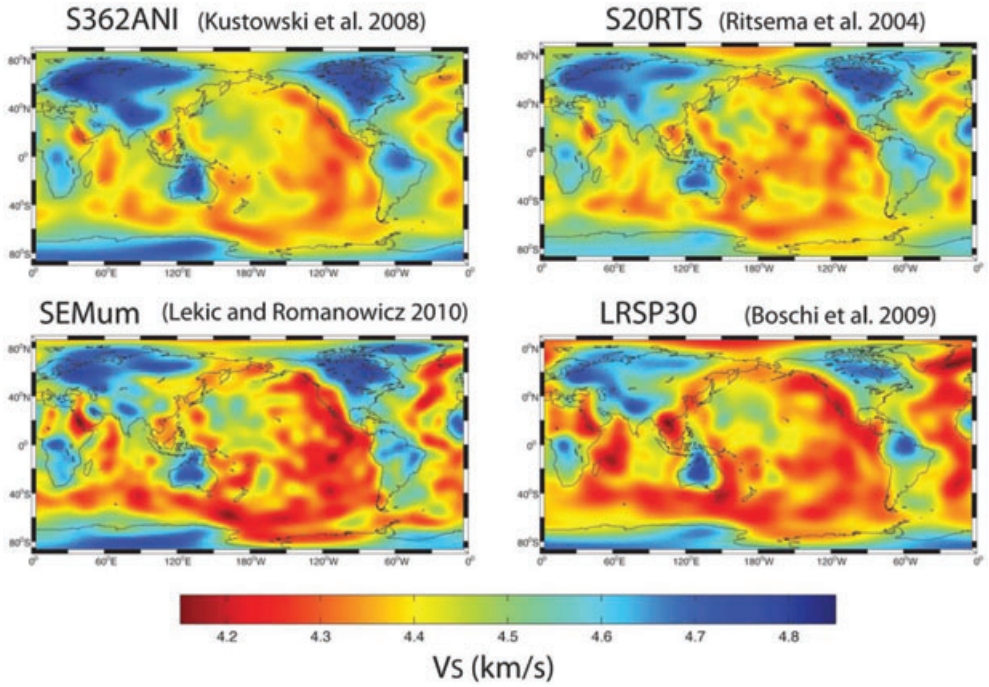

Figure 2. Slices at 150 km depth of four global V_S models. All models are expanded in spherical harmonics up to degree 24.

not represent a problem. Typically, the average structure is often removed and only relative variations are shown. For what concerns the interpretation, however, is important to consider the model as a whole, hence including its average (or degree 0 in a spherical harmonics expansion).

In Fig. 3 , we show the $<V_S(z)>$ of the previous four models plus SAW24ANB (Panning *et al.* 2010). Note that SEMum (Lekic & Romanowicz 2011) is not defined in the transition zone and LRSP30 (Boschi *et al.* 2009) is defined down to 600 km. SAW642ANB and S20RTS are constructed starting from PREM, therefore their averages are characterized by the large 220 km discontinuity of PREM. This discontinuity is not required globally (e.g. Deuss 2009, and references therein) and can be avoided without worsening the fit, as the other models demonstrate. The other three models have a relatively similar variation with depth of the average model in the top 400 km and no 220 km discontinuity. Except for S362ANI, which is slower than the other models in the transition zone (probably due to the choice of adopting a shallower discontinuity between upper and lower mantle, see Fig. 3), the major differences between the averages of the models occur within the first 200 km. It is not the aim of this paper to find out the origin of the differences between available seismic models, but it is likely that the inconsistency in the variation with depth of the models is affected by crustal corrections and trade-off with anisotropy structure (Bozdag & Trampert 2008; Ferreira *et al.* 2010). In addition, it must be recalled that the models have been constructed with different data and regularization schemes. In this sense, the similarity between the models is more remarkable than the differences among them. Nevertheless, in a quantitative interpretation of the models, it is important to clarify how these differences affect the thermochemical structure of the mantle and what are their implications in terms of mantle dynamics.

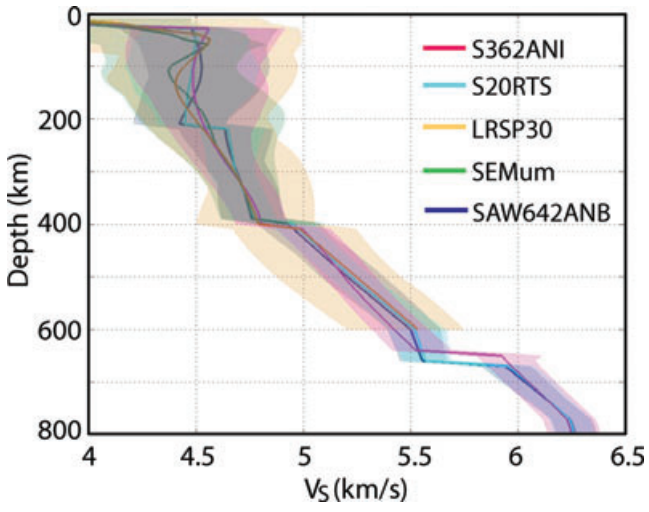

Figure 3. Average depth profiles and maximum range of the anomaly amplitudes of five V_S models, see legend.

3.3.2 Lateral variations

The amplitudes of the lateral variations (ΔV_S) are, in general, less well resolved by seismic data than the degree 0. Different regularization schemes (e.g. choice of roughness and norm damping) are able to strongly modify ΔV_S without altering the data fit much (e.g. Carannante & Boschi 2005). Seismic models shown here (Fig. 3), however, are characterized by similar amplitudes, with a maximum in the first 250–300 km of the upper mantle and a slight decrease in the transition zone (Fig. 3).

3.4 Modelling geoid and topography

The gravitational flow due to the interior density contrasts leads to deformation of the Earth's surface as well as of internal chemical boundaries (such as the core–mantle boundary). The transient, time-dependent viscous relaxation of boundaries (density jumps) in a flowing mantle is characterized by exponential decay times that are

on the order of a few thousand years. Since these timescales are much less than those on which convection displaces the internal density anomalies, we may regard the boundaries as always being in dynamic equilibrium. Therefore, their viscous response to mantle flow can be assumed to be 'instantaneous'.

The instantaneous mantle flow is readily computed with typical fluid-dynamics codes, which solve the equations of highly viscous flow. Our fluid-dynamics code, STAG-YY, uses a finite-difference/finite-volume technique on a staggered grid and computes models in a 3-D spherical shell by using a yin-yang grid (Tackley 2008). The version of the code that we use here is able to handle very large viscosity variations thanks to the implementation of a new pressure interpolation scheme in the multigrid solver (Tackley 2008).

STAG-YY is here used to simultaneously solve the momentum and continuity equations for incompressible, infinite Prandtl number flow. Free-slip boundary conditions have been used. Both inner and outer boundaries are driven by the derived density variations with the specified viscosity structure. Self-gravitating geoid and topography are calculated using the approach introduced by Zhang & Christensen (1993) and also implemented by Zhong *et al.* (2008). The reader is referred to these for full details; a brief summary is given here. In this approach, it is noted that for incompressible flow the gravitational perturbation term in the momentum equation can be absorbed into the pressure term by defining an effective pressure, so the flow solver does not have to be modified. Topography at the surface and CMB, calculated from the normal stress on these (non-deforming) boundaries, together with the 3-D density field are then transformed into spherical harmonics, allowing the surface geoid and corrected (for self-gravitation) topography to be calculated separately for each spherical harmonic degree and order then transformed back into grid space.

Viscosity is central, of course, to mantle dynamics. To focus on the relative differences between different compositional and seismic structure, we use the same viscosity model (and boundary conditions) throughout this paper. The differences between the synthetics fields of geoid and topography are therefore only due to the 3-D density structure. Tests of the same thermochemical with viscosity structures that includes large lateral variations are shown and discussed in supporting material.

4 RESULTS: THERMOCHEMICAL INTERPRETATION OF SEISMIC MODELS

For the sake of simplicity, we find it convenient to discuss separately the absolute T–C values (the degree 0 of the models) from the lateral T–C variations. From what we said before, it should be clear, however, that the latter are strictly linked to the former, contrarily to what happens in purely seismic studies.

In two separate sections, we show how our models determine the thermal lithosphere–asthenosphere boundary (LAB) and we compare our seismically inferred T structures with the thermal structure of oceanic lithosphere according to cooling models.

4.1 Average structure and variation with depth

Given the composition C, the average thermal and density structure, $<T>(z)$ and $<\rho>(z)$ depend on the uncertainties in $<V_S>(z)$ and in the mineral physics properties. In the lower mantle, $<V_S>(z)$ is similar between different models, which suggests that it is relatively well constrained (Cobden *et al.* 2009). The shear properties of the lower mantle minerals, however, have large uncertainties that can affect significantly the degree 0 of the thermochemical model. Unlike the lower mantle, the upper mantle is characterized by relatively small elastic uncertainties, but anelasticity plays a significant role.

We found that the principal source of uncertainty in the radial T–C profiles for the first 250 km is related to the discrepancies between seismic models. In the top 400 km of the mantle, uncertainties in mineral physics parameters do not play a significant role on depth variations of T–C structures (Cammarano & Romanowicz 2007; Cobden *et al.* 2008) (but note that the T profile can be shifted by $\sim\pm$100 K, Cammarano *et al.* 2003). For example, in spite of the large uncertainties in the P–T-dependence of anelasticity, we tested that the radial thermochemical structure changes only slightly when using the same V_S model (and for given elastic properties).

The regionalized thermal and density profiles shown in Fig. 4 reflect the differences in the variation with depth of the seismic models. The profiles are obtained by averaging each 3-D model over all six regions of GTR1 (see Fig. 1, same colour scheme is

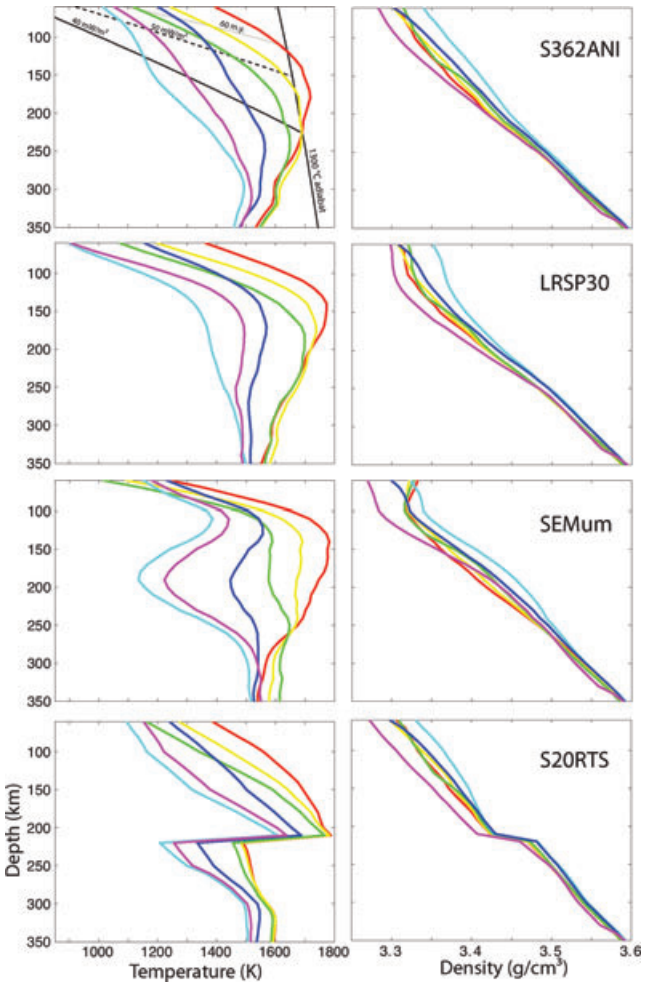

Figure 4. Thermal and density regionalized profiles obtained from the interpretation of different seismic models with the same compositional structure (pyrolite + petrological lithosphere) and based on the reference mineral physics model XSLB08+Q5. Regionalization and colour scheme are as in Fig. 1. For reference, two continental (with surface heat flow of 40 and 50 mW m^{-2}) and one oceanic (60 Myr old) geotherms plus a 1300 °C mantle adiabat are plotted in top-left panel.

applied for Fig. 4). The qualitative aspects that are in common to all the seismic models are:

(1) continental regions are relatively cold down to ∼300 km;
(2) the oceanic geotherms in the shallow upper mantle are gradually hotter moving from old to young oceans and they converge around 250 km;
(3) small ΔT variations are observed below 300 km.

Apart from these features, the shape of the regionalized T and ρ profiles is very different. It is obvious that each set of geotherms would point to a very different dynamical evolution of the mantle. Note that the differences in regionalized geotherms are due partially to the variations in average $V_S(z)$, but also depend on how ΔV_S changes with depth in different tomography models.

In the background of the top panel of Fig. 4, we plot continental and oceanic geotherms for reference. The continental geotherms are purely conductive and we computed them at steady state, based on surface heat flow and radiogenic heat production in the crust (Chapman 1986). The oceanic ones are based on a simple half-space cooling model at different oceanic ages (Turcotte & Schubert 1982). The geotherms obtained with S362ANI, characterized by a smooth decrease of ΔV_S from the top to the base of the lithosphere, are the most consistent with the calculated continental and oceanic geotherms (Fig. 4, top panel). More pronounced depth-dependence of ΔV_S, such as those in SEMum, results in more complicated geotherms. Note also the unrealistic geotherms of S20RTS associated with the 220 km discontinuity of its reference model (the same is true for SAW642ANB, not shown here). The density profiles (Fig. 4, right-hand panels) show less pronounced variations with depth, in agreement with their smaller sensitivity to seismic velocities compared to T (Cammarano *et al.* 2003). All the density profiles are fairly similar below 250 km (Fig. 4).

The compositional effects on T and ρ profiles are shown in Fig. 5. The six colour lines, as for Fig. 4, correspond to the six regions of the GTR1 model (same colour scheme). Thermal and density regionalized profiles in Fig. 5 are obtained from the interpretation of the same seismic model (S362ANI) with a petrological lithosphere (solid lines in top panels) or assuming MM-C2 as radial compositional structure (solid lines, bottom panels). Thermal and density average profiles obtained by assuming pyrolite are represented as dashed lines. The variations between the dashed and the solid lines indicate the role of compositional effects for each of the six regions.

The variations between the two radial compositional structures tested (bottom panels Fig. 5) obviously have a global character (i.e. they occur in all six regions). The thermal profiles change only below 250 km (bottom panels, Fig. 5). On average, the seismic geotherms below this depth are characterized by negative gradients if a pyrolite composition is assumed. T-gradients with depth become slightly positive if we allow C to vary with depth (Fig. 5). These features are consistent with previous findings (Kuskov & Kronrod 2006; Cammarano & Romanowicz 2007; Cammarano *et al.* 2009; Khan *et al.* 2009). On the other hand, density is globally reduced in the first 250 km when an MM-C2 composition is used (bottom panels, Fig. 5). Below 250 km, where the MM-C2 has a strong compositional gradient, the average density gradient with depth becomes more pronounced (Fig. 5). Specifically, $\Delta\rho/\Delta z$ between 250 and 350 km goes from 1 for pyrolite to 1.3 Kg m^{-3} km^{-1} for MM-C2. The ρ gradients in this depth range are very similar, at a given C, for all the seismic models (Fig. 4).

Modelling the petrological lithosphere does not affect the thermal profiles inferred from seismic velocities significantly, but gives a better description of the density structure of the lithosphere (Fig. 5, top panels). As expected, the major decrease in density occurs in the old cratonic areas, that are modelled with a depleted C typical of an average Archean lithosphere (Table 1).

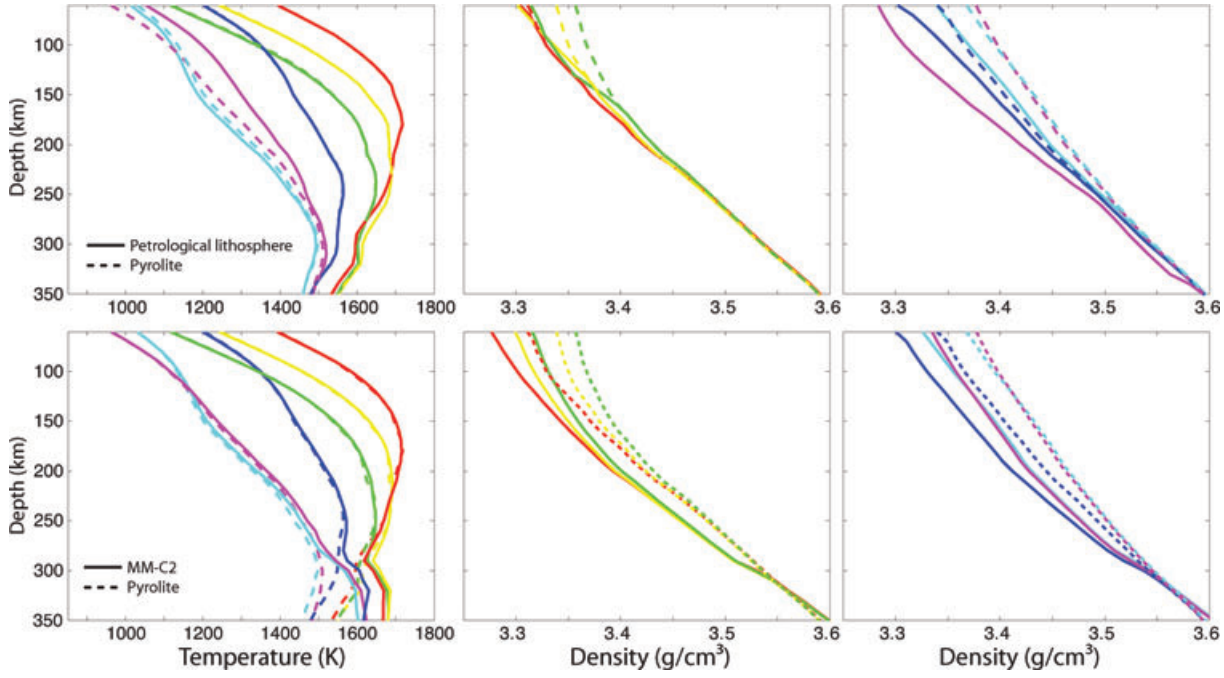

Figure 5. Compositional effects on thermal and density profiles from the interpretation of S362ANI model. Colour scheme of the six regionalized profiles is the same of Fig. 1. Dashed lines refer to thermal and density profiles obtained assuming pyrolite. Solid lines are profiles obtained by including a petrological lithosphere (top panels) or assuming MM-C2 as radial compositional structure (bottom panels). Density profiles are shown separately for oceanic (mid panel) and continental (right-hand panel) regions for clarity.

The variation with depth of the T–C structure in the transition zone is poorly determined. In spite of the general consistency of average seismic velocities within the transition zone, the relative errors in modelling the shear properties of the minerals that occupy subsequent depth ranges within the transition zone (e.g. olivine-wadsleyite and ringwoodite) introduce a large source of uncertainty (Cammarano *et al.* 2005a).

4.2 Lateral variations

Relatively small differences between velocity models (Fig. 2) can translate into dynamically important thermal and density variations (Figs 6 and S7, respectively). T variations between tested models are in the order of ∼400 K in cold, continental areas and of ∼150 K in hot, oceanic regions (Fig. 6). The effect is smaller in hot areas, where anelasticity causes a given ΔV_S to be explained by a smaller ΔT (Cammarano *et al.* 2003).

Uncertainties in the elastic properties, which have been assessed by Cammarano *et al.* (2003), modify the estimated temperatures by ±100 K at this depth. Note that they only affect the average value of temperature at each depth, but not its lateral variations. The larger uncertainties on ΔT from mineral physics are, therefore, related to uncertainties in anelasticity. From extreme anelasticity models based on the Arrhenius law (see eq. 1), we found that T in hot areas can vary between −150 and +75 K at 150 km depth (see Fig. S8 in Supporting Information), where the effect of Q is highest. Intrinsic T-dependent attenuation has practically no effect in cold, continental areas at this depth.

Introducing lateral C variations does not change much the thermal interpretation of seismic models, but gives a more realistic density structure. Modelling a petrological lithosphere, for example, gives cratonic T at 150 km that are only 100 K hotter (corresponding to 20 per cent of the total ΔT) than those obtained assuming pyrolite (Fig. 5), but density is ∼ 0.1 g cm^{-3} lower (around 140 per cent of the total $\Delta\rho$; see Fig. 5).

Finally, lateral thermochemical variations of the transition zone are complicated by effects due to mineralogical phase transformations. To reproduce realistic lateral variations in T and ρ, we neglect seismic results near the depths of phase transitions (380–420 km and 650–780 km depth), where we estimate T simply by interpolation of values found above and below. We also construct models which preserve the sharp character of the mineralogical transitions, replacing or not $<T>(z)$ with a reference adiabatic profile at a potential T of 1300 °C. Since $<T>(z)$ is not well constrained within sharp phase transitions, testing its effect is important for future studies concerning the seismic signature of those phase transitions. However, the effect on geoid and topography is negligible.

4.3 Lithosphere–asthenosphere boundary

Because of the uncertainties in absolute T due to mineral physics and in the variation with depth of seismic models, we have only a very approximate indication of the possible thermal LAB. Variations in composition, as discussed, have a negligible effect. In Fig. 7, we show the variations of thermal LAB inferred from two seismic models (S362ANI and LRSP30) and for two isotherms (∼1000 °C and 1200 °C). In spite of the large local variations between the LAB thicknesses, all of them reproduce the general expected features. Specifically, a thick continental LAB and an age-dependent, shallow oceanic LAB. Our 'seismic' TBLs of continental lithosphere are overall consistent with published models (Artemieva 2009).

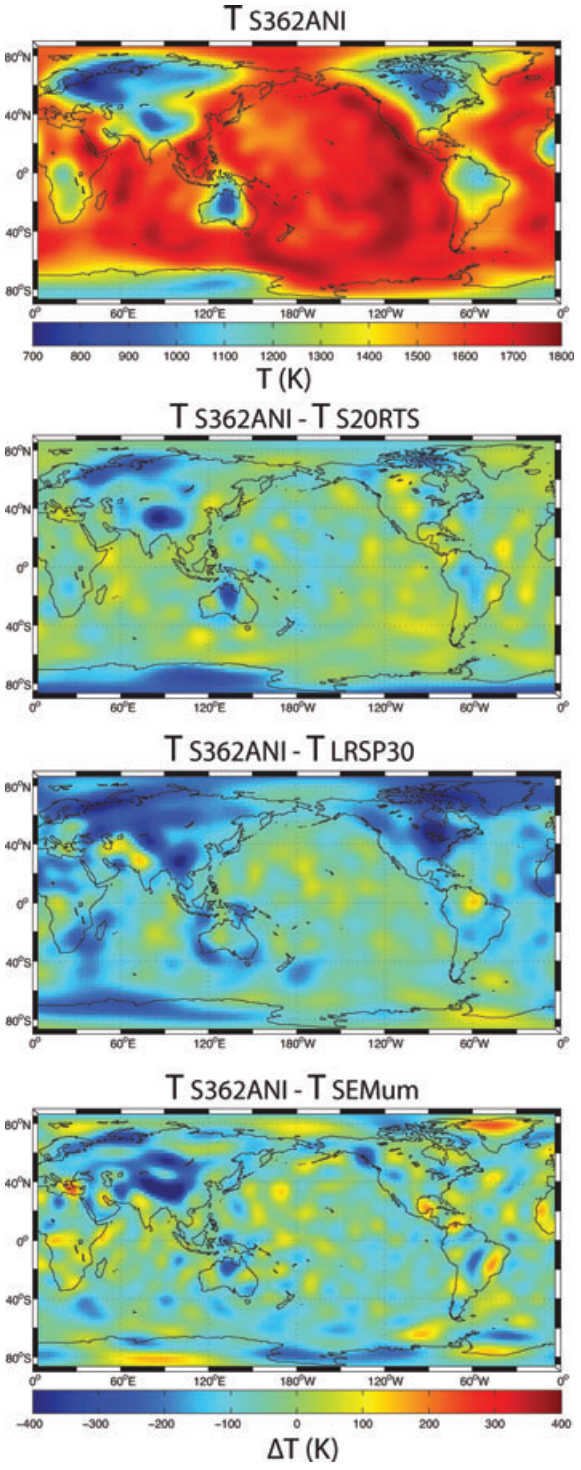

Figure 6. Thermal interpretation at 150 km of the V_S models assuming pyrolite and using the mineral physics model XSLB08+Q5 (see text). Top panel shows absolute T for S362ANI model. Relative variations with T inferred from other seismic models are illustrated in the other panels. All maps are expanded in spherical harmonics $\ell = 0$–24.

In this study, we use the thermal LAB to model the depth of the petrological lithosphere (or CBL), used for our compositional modelling. We are indeed principally interested to model the continents–oceans dichotomy. We anticipate that to clearly separate effects due to variations between seismic models from

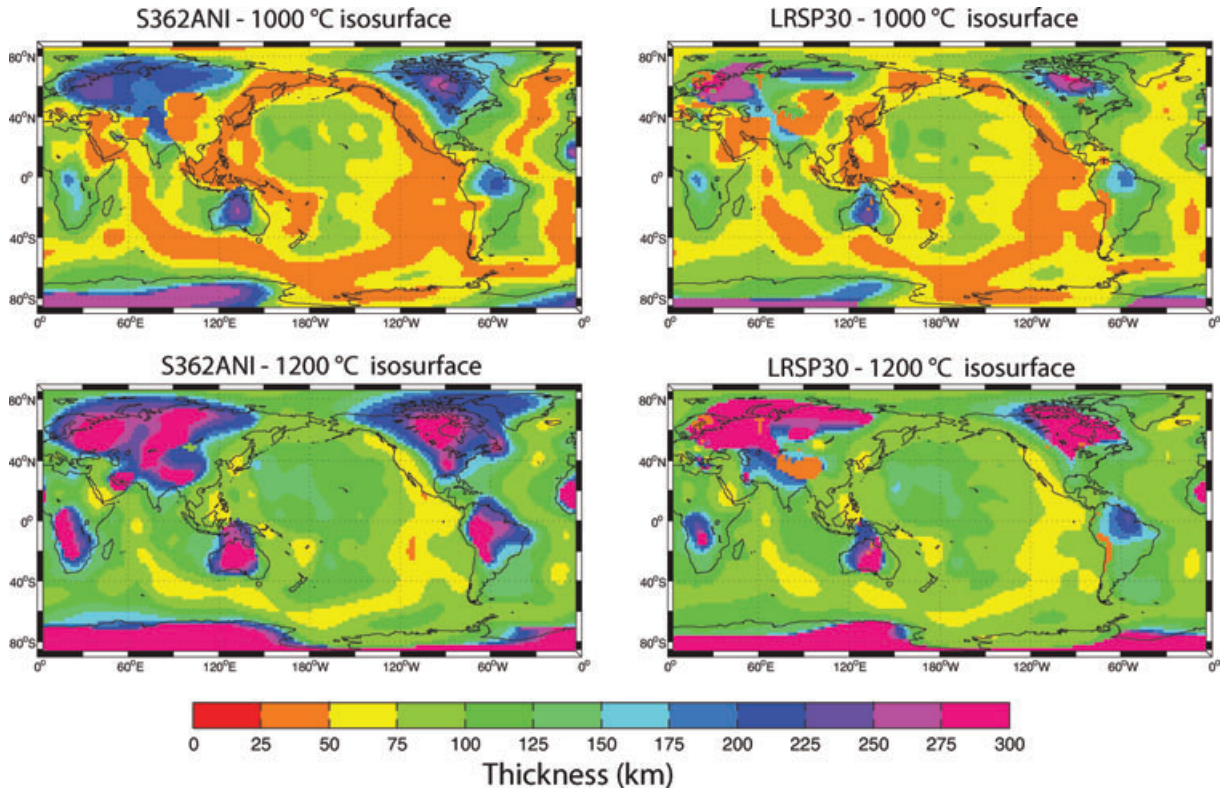

Figure 7. Isosurfaces at 1000 °C and 1200 °C for S362ANI and LRSP30 (the most different in lateral T variations, see Fig. 6). The thermal lithosphere–asthenosphere boundary (LAB) is expected at ∼1100 °C–1200 °C.

compositional ones, we compare thermochemical models with exactly the same petrological lithosphere. The reference LAB is given by the 1200 °C of the thermal model obtained from S362ANI, assuming a pyrolite composition.

4.4 Thermal structure of oceanic lithosphere

The temperature structure of the oceanic lithosphere is one of the better understood geophysical phenomena related to plate tectonics. New lithosphere is created at constant T at mid-ocean ridges and cools with age. Simple models, such as the half-space cooling model or a plate cooling model are very successful at providing an accurate description of the variation of topography and heat flow with age (e.g. Turcotte & Schubert 1982; McKenzie *et al.* 2005, and references therein).

The thermal models obtained from seismic interpretations agree qualitatively with an age-dependent relation. To verify to what extent such a thermal structure is reproducible from seismic models, we compare the inferred T structures as a function of the age of the oceanic crust (we use the model of Müller *et al.* 2008) with the structure predicted by a half-space cooling model. Reversely, based on the theoretical T structure, we also computed the seismic (and density) structure by using the same mineral physics model (XSLB08 +Q5). (Fig. 8, plus Figs S9 and S10 in Supporting Information).

None of the seismically inferred models is able to reproduce sufficiently well the theoretical thermal structure (Fig. 8). In general, the T structure inferred from observations is smoother than what predicted by cooling models (Fig. S9). This is not surprising, in view of the limited resolution of surface waves or of the long-period waveforms used in global studies.

However, there is one aspect that all the seismic models share. Their minimum velocity below younger oceans is around 100 km and all seismic models are faster (from a minimum of 0.5 per cent up to ∼3.7 per cent) at 50 km (Fig. 8). This is in conflict with classical cooling models that naturally predict V_S to be minimal at much shallower depth beneath mid-ocean ridges (Fig. 8, but also Figs S9 and S10).

Another difference between the seismic models and the cooling one concerns how the lateral variations in V_S change with depth (Figs 8 and S10). ΔV_S predicted by the cooling model at 50 km are much larger than ΔV_S at 100 km. The seismic models, instead, have similar ΔV_S at these two depths (Figs 8 and S10).

4.4.1 Discussion on the nature of the oceanic mantle

The systematic decrease in V_S beneath mid-ocean ridges is an interesting feature that deserves an extensive discussion. Is it real? And, if so, what could be its origin?

The inconsistency between the seismically inferred thermal structure of the oceanic lithosphere and the well-accepted model of its evolution led already some authors (i.e. Priestley & McKenzie 2006) to formulate a semi-empirical relation that links the two. They avoid, this way, using mineral-physics-based relations between seismic velocities and T. Forcing a seismic model to follow the theoretical expected T structure does not resolve the paradox of this inconsistency. We agree, however, that part of the problem can lie in the way material properties are modelled.

The decrease in seismic velocity from 50 to 100 km beneath ridges and younger oceans cannot be explained by uncertainties in phase equilibria and elasticity. According to cooling models,

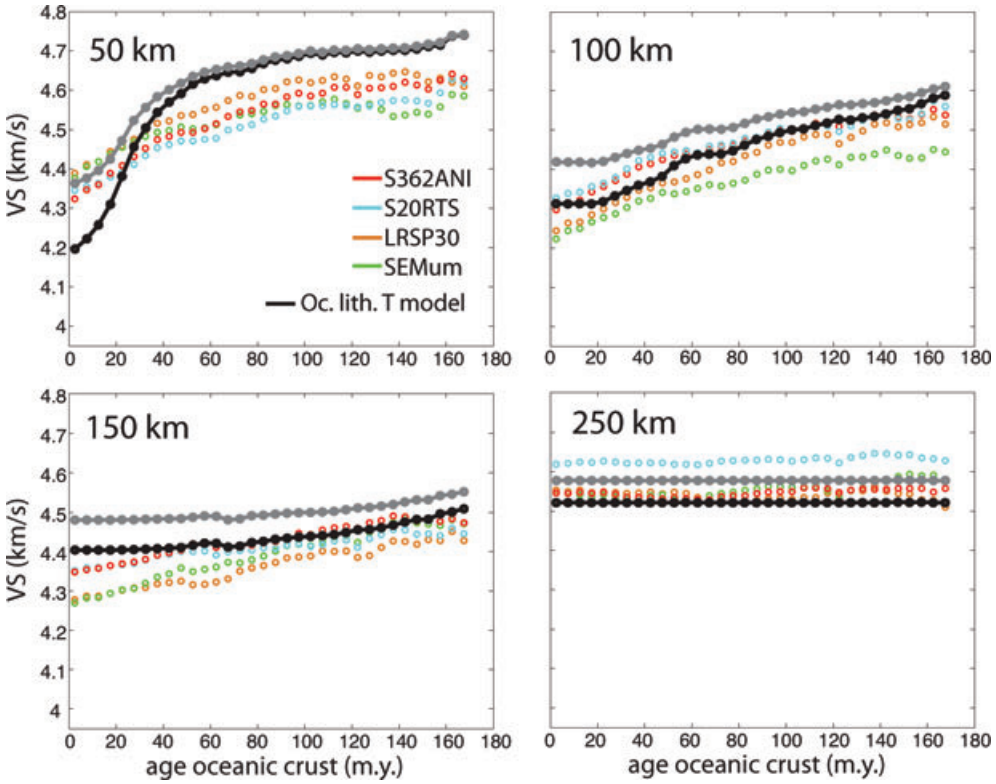

Figure 8. V_S profiles as a function of age of oceanic crust (Mueller *et al.* 2008) at four different depths. In black, the predicted V_S based on a T structure of oceanic lithosphere obtained with a half-space cooling model. To convert T to V_S, we assume pyrolite and use the mineral physics model XSLB08 + Q5. Purely anharmonic values (i.e. without Q effects) are shown in grey. Full V_S and T structures as a function of age plus regional depth-profiles at different oceanic age are shown in Figs S9 and S10 in the Supporting Information.

the increase in temperature is negligible between these two depths (we are below the lithosphere). Therefore, purely elastic velocities should increase with depth, when a uniform chemical composition is assumed.

The strong T-dependence of anelasticity makes even more problematic to explain the high V_S beneath ridges. The elastic velocities should be further reduced because of Q when temperatures are approaching the solidus. Interestingly, constraints on observed seismic attenuation (Romanowicz & Mitchell 2007) and T-dependence of anelasticity (both taken into account in our Q5 anelasticity model) are able to better reproduce seismic velocities below ∼70–80 km depth (Fig. 8). A possibility is that the mechanism that is responsible for intrinsic attenuation below 70–80 km is not active at shallower depths. If we do not introduce any additional compositional complication, it is very difficult to imagine why this should happen. Surely, there should be another or other factors than temperature that prevails on the anelastic corrections. We may conclude, therefore, that, if this discrepancy is real, an additional compositional factor is required to reconcile cooling models with seismic observations.

The global seismic models here analysed do not yet provide conclusive evidence for such a discrepancy. Surface waves and long-period waveforms used in global studies have a horizontal resolution on the order of hundreds of kilometres. In any case, this is clearly sufficient to capture the main long-wavelength features of thermal structure (Fig. S9, Supporting Information). However, their vertical resolution, which is on the order of ∼50 km, might be inadequate. The starting model, crustal corrections and regularization schemes that enter into the solution of the linearized inverse problem are also an issue. For example, the variations of V_S with depth depends 1) on the starting reference model and 2) on a subjective choice of damping, which can be depth-dependent and accounts, as much as possible, for the different resolution with depth of seismic data used. Tuning the damping factors at different depths based on physically expected ΔV_S and/or using starting models that have a physical meaning (Cammarano & Romanowicz 2007; Romanowicz 2009) should be able to improve the physical character of the seismic models. Alternatively, non-linear procedures can be used to measure the reliability of several given models (Tarantola 2006; Khan *et al.* 2011).

In this study, we reverse the question, asking: to what extent does the seismic structure predicted by a cooling model deteriorates the fit of surface waves? For all seismic models considered here, we replace the oceanic lithosphere with that predicted by a half-space cooling model. We compute the variance reduction of Love and Rayleigh wave data (Visser *et al.* 2008), assuming PREM anisotropy in all cases, and compare the values with those achieved by the original models. The variance reduction slightly decreases when forward seismic structure consistent with a thermal model is used, but the difference is not significant compared to the variance reduction associated with different seismic models.

More systematic tests and regional seismic studies are required to give a robust evidence of the variations of V_S beneath young oceans. Nevertheless, all seismic studies to-date, including regional ones (e.g. Harmon *et al.* 2009, for the East Pacific Rise), show the same trend. Very interestingly, the same group Yang *et al.* (2007) found also a considerably low attenuation, picking up around 40 km depth, beneath the East Pacific Rise.

If seismic observations are confirmed, an attractive hypothesis for reconciling them with cooling models is the one suggested by

Karato (1986) and expanded in Karato (2008). The idea consists of a feedback mechanism between partial melting, water content and their effects on physical properties. Partial melting occurring at a depth around 65 km beneath ridges would remove all water from mantle rocks. The presence of a small amount of partial melt will hardly have an effect on seismic velocities [it is estimated that is necessary to have a fraction higher than 1 per cent to produce significant effects on seismic velocities (Hammond & Humphreys 2000)] and would tend, in any case, to reduce seismic velocities and viscosity. In its rheological model of oceanic lithosphere, Karato proposes that the top part of the mantle (above 65 km) is dry, and thus highly viscous and seismically fast. On the other hand, the presence of small amount of water below 65 km would soften the material significantly and reduce the seismic velocities, mostly because of water-enhanced anelasticity effects. In spite of the poor knowledge of the effects of water on seismic properties and anelasticity in general, we find that this hypothesis represents a likely explanation for the observed discrepancy. It is interesting to note, finally, that the Karato's hypothesis was first conceived as a rheological model (Karato 1986).

Additionally, or alternatively, the origin of the decrease in velocity may be searched in non-monotonic compositional variations within the upper mantle, also these regulated by partial melting. An important role in determining the seismic velocities at (relatively) shallow depths may be played by the plagiocase-spinel transition, plagiocase being slow ($V_S \simeq 3.5$ km s^{-1} at 50 km and 1200°) and spinel fast ($V_S \simeq 5.0$ km s^{-1} at the same conditions). The transition occurs around 80 km for pyrolite, but it is pushed upward for very depleted composition (Borghini *et al.* 2010). An overall depleted, harzburgitic upper mantle (well below the lithosphere in proximity of mid-ocean ridges) can therefore get significantly higher velocities at ∼50 km depth (around 4–5 per cent for V_S) compared to normal mantle composition if spinel is stable over plagiocase. To explain the reduction of V_S below this depth (in absence of a sensible T variation), plagiocase should be stable again, which implies having an undepleted composition. Owing to multiple episodes of melt depletion and secondary melt-impregnation, there is poor knowledge of the mineralogy of pristine mantle. Most lherzolite massifs, indeed, represent secondary (refertilized) rather than pristine mantle (e.g. Roux *et al.* 2007). Note that harzburgite and pyrolite V_S below the plagiocase-spinel transition (around 80 km for pyrolite) are very similar (harzburgite is faster by ∼0.3 per cent).

5 RESULTS: TESTING $T-C$ MODELS WITH GEOID AND TOPOGRAPHY

All the results shown in this section are based on the viscosity profile V1 of Forte *et al.* (2010) and on free-slip boundary conditions. The overall good fit to geoid of the seismically inferred ρ models (Figs 9 and 12) shows their mutual consistency. The fact that one of these models fits the geoid better than another, however, does not prove that it is a 'better' model. In principle, for each of the density structures used it would be possible to tune the viscosity profile to get the same misfit. In other words, due to the trade-off between viscosity and density, the best-fit models of geoid and topography should always be thought as density+viscosity models.

5.1 Effects of compositional structures

In Fig. 9, we illustrate the relative effects of the compositional structures. For any observed field N^O and computed fields N^S, the cumulative variance reduction, given by

$$\chi = 1 - \frac{\sum_{\ell m}(N^O - N^S)^2}{\sum_{\ell m}(N^O)^2} \tag{3}$$

is computed by expanding N^O and N^S in spherical harmonics from the lowest degree ($\ell = 2$) to the same upper degree, (maximun is $\ell = 24$), on a regular $2^\circ \times 2^\circ$ grid.

We also plot the variance reduction at each degree ℓ by directly comparing the spherical harmonics coefficients, that is,

$$\chi_\ell = 1 - \frac{\sum_m((a_m^O - a_m^S)^2 + (b_m^O - b_m^S)^2)}{\sum_m(a_m^{O\,2} + b_m^{O\,2})}, \tag{4}$$

where a_m and b_m are, respectively, the harmonic coefficients for cosine and sine terms at a given degree ℓ. A perfect fit gives a value

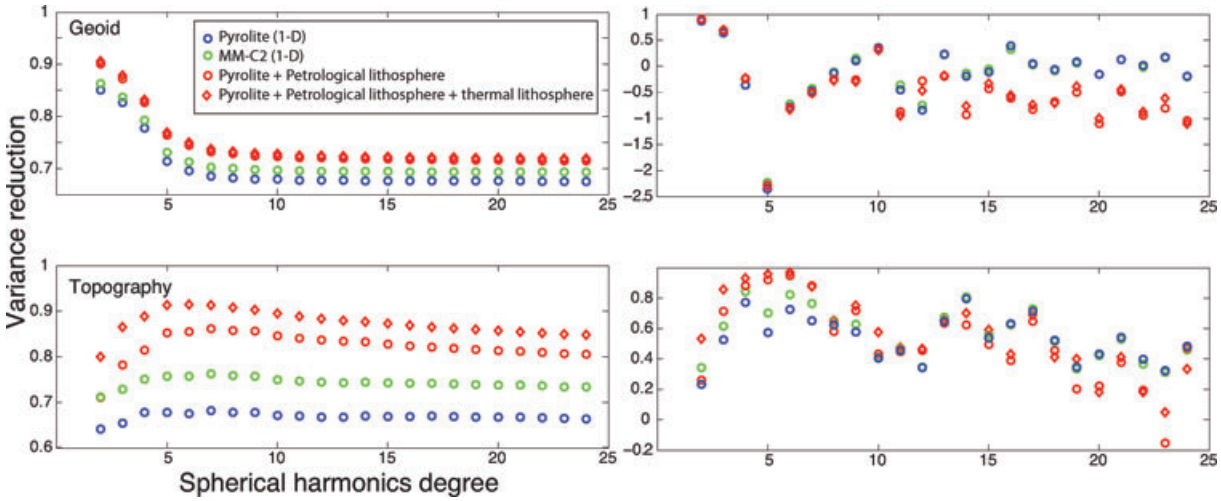

Figure 9. Cumulative variance reduction (left-hand) and for each ℓ (right-hand panels) for geoid (top) and topography (bottom panels) of 3-D density models obtained from the T interpretation of S362ANI for several compositional structures (see legend and text). All densities are obtained by using the reference mineral physics model (XSLB08+Q5). Viscosity profile is V1 (Forte *et al.* 2010).

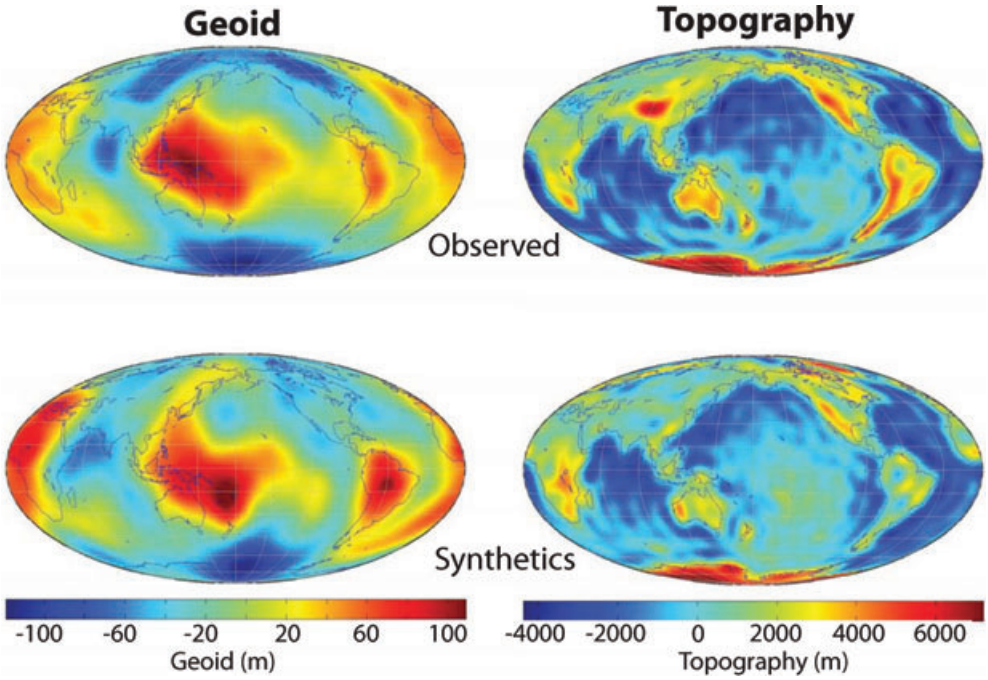

Figure 10. Observed (top panels) and synthetic (bottom) geoid and topography for $\ell = 2$–24 on a Mollweide equal area map projection. The observed non-hydrostatic geoid is obtained from the GGM02 gravitational potential field, and the topography model is ETOPO5. Synthetics refer to the 3-D density model inferred from the thermal interpretation of the S362ANI V_S model using the mineral physics model XSLB08+Q5 (see text), and assuming pyrolite plus a petrological lithosphere (see text). Viscosity structure is given from the V1 profile from Forte *et al.* (2010). The variance reduction computed for this case is given in Fig. 9 (see red circle at $\ell = 24$).

of 1 in both cases. The observed non-hydrostatic geoid is obtained from the GGM02 model of the gravitational potential field (Tapley *et al.* 2005) after removing the hydrostatic oblateness due to the rotation of the Earth. Topography is ETOPO5 (from NOAA, National Geophysical Data Center). An example of the computed geoid and topography compared to the observations is shown in Fig. 10. In general, the principal features of both geoid and topography are reproduced quite well.

The cumulative χ of the geoid tends to become horizontal as ℓ grows (top-left panel, Fig. 9), consistent with the concentration of a large part of the signal at long wavelength (low ℓ). It is therefore particularly important to fit the lowest degrees, especially the degree 2 that has the maximum power content. This is also the case for topography, although the maximum power is observed at degree 3 and the spectral distribution is relatively more homogenous compared to the geoid.

All the synthetics of Fig. 9 are based on the same seismic structure (S362ANI) and on different C structure. The 3-D density structures, therefore, couple the purely C effects with the inferred (slightly different) temperatures. All the models are only different in the upper mantle (down to 660 km) and have the same crustal structure (CRUST2.0). Hence, the relative variations reflect the effects due to upper-mantle structure only. Modelling the 3-D compositional variations within the lithosphere improves the fit of both geoid and topography (Fig. 9, left-hand panels). Interestingly, the pattern at each degree indicates that our petrological lithosphere deteriorates the fit when moving to shorter wavelengths (right-hand panels). Perhaps, this could be partially associated with our simplified compositional parametrization, but we note that this specific result is linked to the used viscosity structure and to the boundary conditions (free-slip) used. Our result shows the importance of considering the full effects on the geoid (i.e. also the lowest ℓ). For instance, if we neglect the first 6 degrees of the geoid when studying the global effect of the petrological lithosphere, we would interpret the results in the completely wrong way. Note also that our result is consistent with the analytically computed geoid kernels for the specific viscosity profile used (assuming free-slip conditions). For example, the geoid kernel at $\ell = 2$ has a positive opposite sign at upper-mantle depths, whereas the kernel at $\ell = 8$ is negative.

To better understand the origin of the opposite effects of the petrological lithosphere at long and (relatively) short wavelengths, we map its effects on geoid and topography including or not the first three harmonic degrees (Fig. 11). In the oceans, long-wavelength structure is dominant and therefore the improvement of the fit observed in Fig. 9 is mostly related to oceanic signature. Within continents, shorter wavelengths become dominant. Modelling the low-density cratonic roots pushes the geoid up by $\sim$10 m (Fig. 11), indicating that the dynamical contribution exceeds the static one. And this results in worsening the geoid fitting.

Topography has an opposite effect compared to geoid between oceans and continents. The oceanic topography is still dominated by very long wavelengths and has a negative sign, that is, topography decreases where geoid becomes higher in the oceans (Fig. 11, top panels). On the other hand, continents become significantly higher when a petrological lithosphere is modelled and, at the same time, the geoid becomes higher too, as just discussed.

Rigid (non-deformable) continents should be more appropriate. However, even when we use typical T-dependent viscosity laws (see supporting material), continents are still too weak compared to what is required from gravity data. Variation in composition, such as dehydration of the deeper part of the continents, could contribute to increase their viscosity further. This hypothesis, indeed, has already been postulated to explain the long-term stability of continental roots (Karato 2010). We increased the viscosity of

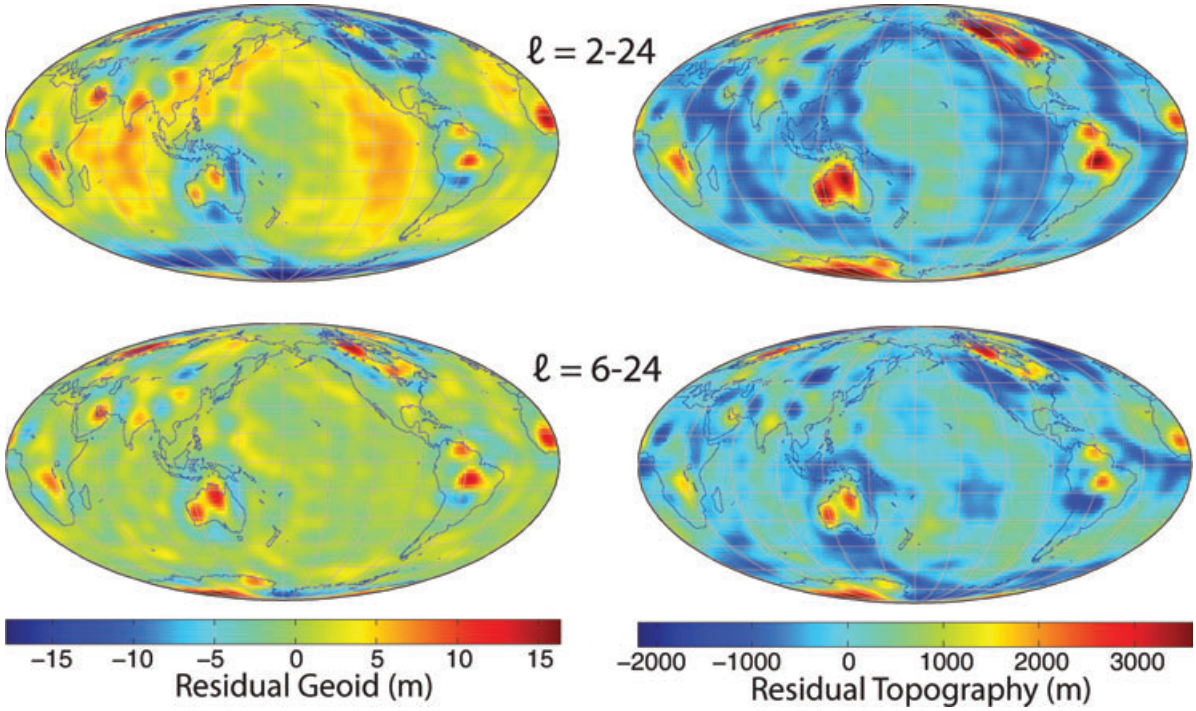

Figure 11. Effect of petrological lithosphere on geoid (left-hand panels) and topography (right-hand). The residuals (values model A–model B) are due to the difference in the density model by converting to T the same seismic model (S362ANI) with (model A) or without (model B) a petrological lithosphere. Viscosity is always given by the profile V1 (Forte *et al.* 2010). Bottom panels exclude the very long wavelength structure. Colour scale is 15 per cent (50 per cent) of total spatial geoid (topography) variations.

continental lithospheric blocks up to three orders of magnitude, but effects on geoid and topography are still limited and do not eliminate the discrepancy (see supporting material).

The only other option to reconcile the continental signal with gravity data is to reduce their chemical buoyancy (i.e. increase their density at given P–T conditions). Therefore, our result indicates that the composition of the lithospheric mantle is less depleted, on average, of what here used. Our result is consistent with (Forte & Perry 2000) and shows the potential of gravity data for determining composition.

Using MM-C2 instead of pyrolite as an average composition of the upper mantle hardly affects the $\ell > 10$ structure (Fig. 9). However, the overall effect (governed by the very long wavelengths) is only slightly smaller compared to that of the petrological lithosphere. The general spatial pattern, shown in Fig. S13 of Supporting Information, is only slightly modified. Note that, in this case, the density variations between the models are not only confined in the lithosphere.

In Fig. 9, we also show that implementing a forward thermal structure of the oceanic lithosphere instead of the 'too smooth' seismically inferred thermal structure better satisfies the topography, while there is practically no effect on the global geoid.

5.2 Effects of differences in seismic models

We show in Fig. 12 how the differences between the seismic models affect geoid and topography. All the computed synthetics are based on 3-D density structure inferred by the thermal interpretation of the seismic models with the same compositional structure (in this case pyrolite plus a petrological lithosphere) and using the same mineral physics model (XSLB08+Q5). Except LRSP30, which is defined down to 600 km and smoothly merged to S362ANI below this depth, the other three seismic models are defined throughout the mantle. We dot not show results for SEMum, which is only defined in the top 400 km of the upper mantle. To isolate the effects due to upper-mantle structure, we assume the same thermochemical structure for the lower mantle for the models shown in the mid-panels of Fig. 12. Specifically, we use the T-ρ structure obtained by using S362ANI and pyrolite. Geoid and topography for full mantle models and for variations limited to the top 380 km are also shown (in left-hand and right-hand panels, respectively) to illustrate the effects with depth.

As expected, the geoid is not very sensitive to the top part of the mantle (top-right panel of Fig. 12). Variations between seismic models are very small, compared to the compositional effects (Fig. 9). Surprisingly, however, the variations between the seismic structure in the transition zone have an effect that is comparable to that related to variations in whole mantle structure (compare mid and left-hand panels of Fig. 12), starting from degree 2. Topography, on the other hand, is more sensitive to the variations in the top of the mantle (note that we use always the same crustal structure). However, the variations in topography fit between different seismic models are not very large (Fig. 12).

To highlight the spatial variations of geoid and topography between different models, we show the residual with respect to S362ANI, used as reference (Fig. 13). The range of variations between the computed geoids amount to almost 50 per cent of the total observed variations, that is, the min-max geoid values (in contrast, variations due to petrological lithosphere amount to 15 per cent). In general, the variations between the models do not occur in the same places. Each model is, somehow, different from the others. It is remarkable, for example, that some anomalies are found only for one model and not imaged for others. This is the case, for example, with the geoid-low of LRSP30 (a positive sign in our residual geoids) in Siberia or the geoid-high in the East-Pacific off

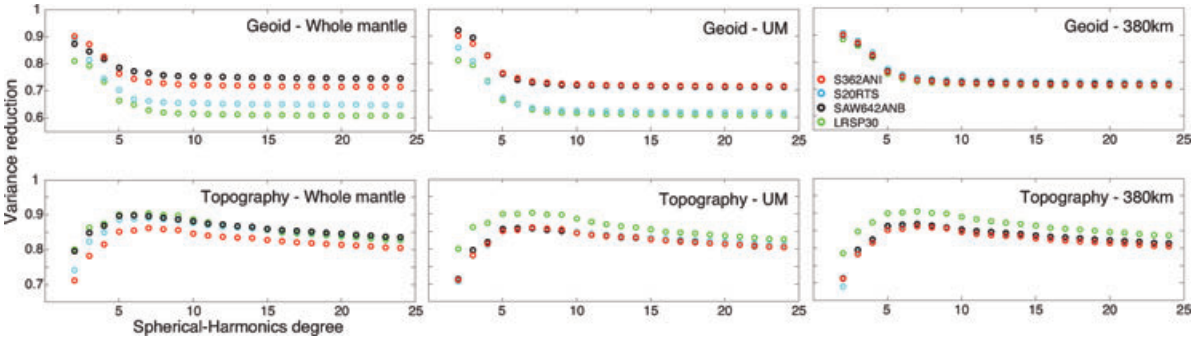

Figure 12. Variance reduction for geoid and topography of 3-D density models obtained from the thermal interpretation of different V_S models for the same given C structure (pyrolite + petrological lithosphere) and using the same mineral physics model (XSLB08+Q5). Viscosity profile is V1 (Forte *et al.* 2010). All the models have the same crustal model (CRUST 2.0, Bassin *et al.* 2000). Left-hand panels show the results for whole mantle models. In mid and right-hand panels, all the models have the same density structure (inferred from S362ANI) below 670 and 380 km, respectively. Correlation coefficients and variance reduction for each ℓ are given in supporting material (Fig. S11, Supporting Information).

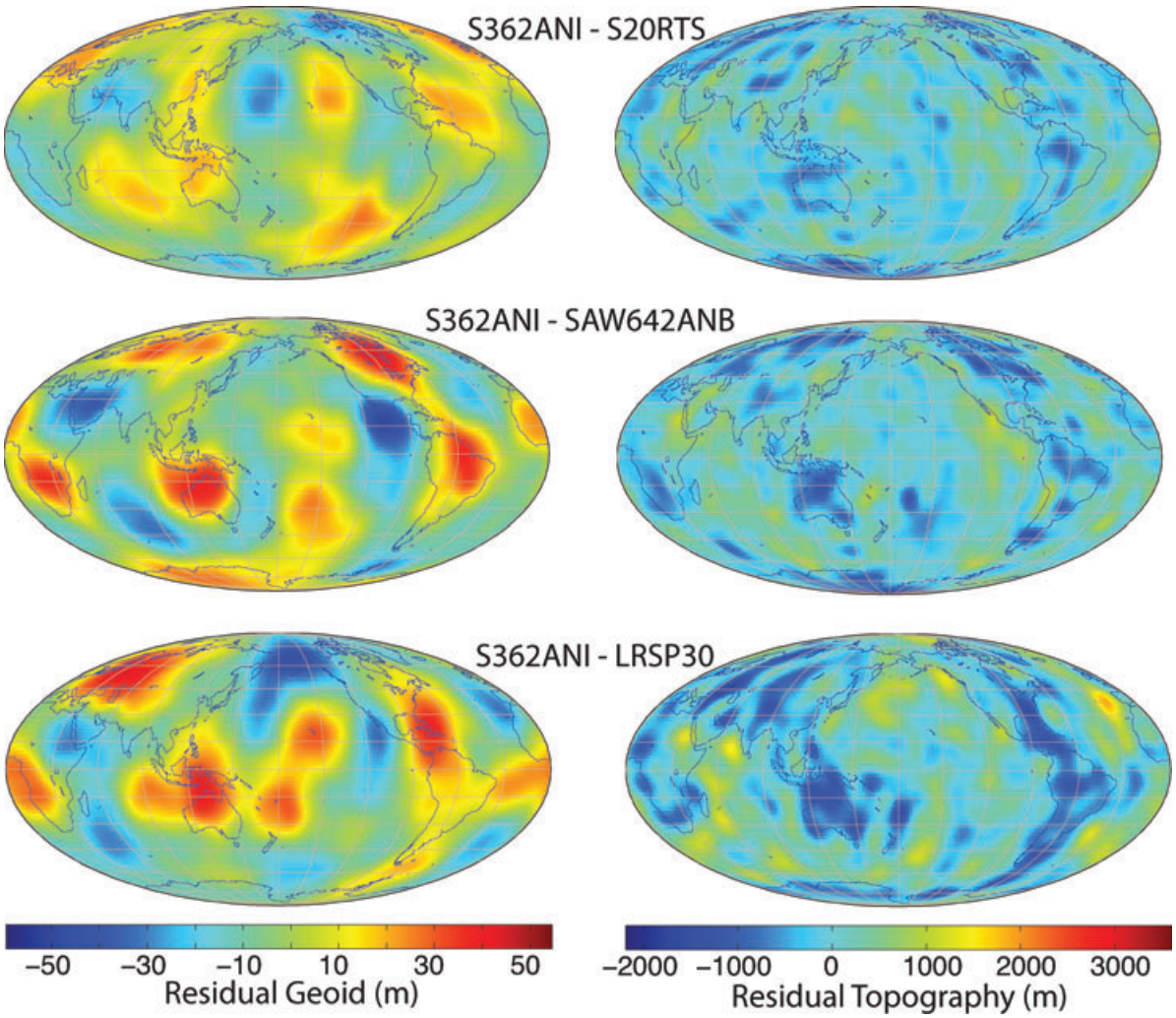

Figure 13. Effect of uncertain upper-mantle seismic structure on geoid (left-hand panels) and topography (right-hand panels). The residuals are due to the difference in density model between the thermal interpretation of S362ANI, used as a reference, and other models, assuming the same compositional structure (a petrological lithosphere + pyrolite below lithosphere). Viscosity is the profile V1. Colour scale is 50 per cent of the total spatial geoid and topography variations.

Central America predicted by SAW642ANB. Interestingly, the major differences occur in complex tectonic areas, such as near the subduction zones of Indonesia and Caribbean (e.g. LRSP30 predicts relative geoid-lows), or in Hawaii (LRSP30 has a low value that it is missing or perhaps displaced in other models). Differences in topography (right-hand panels of Fig. 13) are also fairly large and follow a simpler pattern. LRSP30 and SAW642ANB predict more elevated continental areas than S362ANI.

As we have seen that variation with depth between seismic models is highly variable (in Fig. 3) and that this translates into very different thermal and density profiles (Fig. 4), we also tested what would be the indirect effect of considering the same reference thermochemical (and thus density) profile for all the seismically inferred models. Specifically, we use a reference thermal structure, that is, a 60-Myr-old oceanic geotherm plus a 1300 °C adiabat below the lithosphere and pyrolite composition (MM-C2 has been tested as well). This way, we replace $<\rho>(z)$ with the density profile obtained from a reference thermal structure and we slightly modify the density contrasts according to the new reference temperature. Somehow, we are testing now only the differences in lateral variations between seismic models. In general, the results do not change much (see Fig. S12, Supporting Information). Both geoid and topography are slightly better satisfied. Only the fit of LRSP30 becomes slightly worse when its average is replaced with the reference one.

6 FUTURE DIRECTIONS

In spite of the recent advances in global seismology, fitting gravity data using density distributions derived from seismic models is extremely difficult. As we have shown, this does not depend only on our lack of knowledge of the Earth's viscosity structure, or on the uncertain relation between seismic velocities and density. The discrepancies between geoid and topography maps derived by available seismic models of the upper mantle, indeed, are more important, and significant even at the lowest harmonic degrees. Furthermore, seismic data have an intrinsic limited resolution that has an effect on the geodynamical constraints. If we relax the uncertainties in the elasticity and anelasticity of mantle rocks, (hence the relation between seismic velocities and density), and the large uncertainties in viscosity, including its lateral variations, the problem of determining the thermochemical structure of the upper mantle becomes extremely complicated.

Typical linearized inversions (Simmons *et al.* 2010) are, in our opinion, an inefficient way to improve our current knowledge for the upper mantle. Owing to the increasing computational power, fully non-linear approaches (e.g. Khan *et al.* 2011) are probably better suited. This way, it is possible to test a large family of thermochemical models, independently, against several types of seismic data, gravity data and other geophysical observables (e.g. electrical conductivity). A statistical analysis of the results may elucidate which features are better resolved and which are not. The results can help, simultaneously, to achieve a better understanding of the thermochemical structure of the mantle and point out possible problems with the physical properties modelled. In this sense, our method intends to use the Earth as a laboratory to test a physical hypothesis (here, as a physical hypothesis we mean a set of material properties modelled as a function of $P - T$ and C).

This paper is our first study in this direction, providing a family of thermochemical models that can be used for further testing with other geophysical measurements.

In this paper, we deal uniquely with the isotropic part. Anisotropic effects, which are seismically important, may be modelled by mantle flow, in principle (Long & Becker 2010). Specifically, if the crystals align in the direction of the flow, the resulting anisotropy (called, in this case, lattice-preferred orientation or LPO) can be quantified on the basis of measured mineral properties (Karato 2008). Combined studies of mantle flow and seismic anisotropy already produced important insights, for example, on the mobility of crustal microplate related to mantle flow (Boschi *et al.* 2010; Faccenna & Becker 2010). In the future, it will be possible to extend our approach to obtain fully anisotropic models. In principle, the thermodynamically consistent model we use is already formulated to account for the full elastic tensor and the mantle flow can be already modelled accounting for rigid plates and weak plate boundaries by using our fluid-dynamics code. At the moment, uncertainties in the anisotropic response of minerals and rocks at mantle conditions are still large (e.g. Wenk & Houtte 2004; Karato *et al.* 2008). In any case, our approach may be already extended to test available first-order LPO models of main upper-mantle minerals.

Another aspect of our procedure that can be improved regards the compositional parametrization. The aim of this paper is to produce first-order 3-D compositional models based on petrology and supported by geoid and topography observations at a global scale. For our purposes, we simplify the compositional structure of the lithospheric mantle as much as we can, and we assume no compositional variation below the lithosphere. In recent years, there has been a significant effort to gather and analyse xenolith samples worldwide (Griffin *et al.* 2009). The petrological information on the composition of the subcontinental lithosphere is much more detailed than what we assumed in our 'first-order' model. Its implementation will be particularly important when moving from global to regional and local scales. For example, we did not model any compositional variation with depth within the continental lithosphere, contrary to what observed in typical xenolith data. Indeed, metasomatism is able to refertilize the deeper part of Archaean provinces, leaving a pristine composition in the top part (Griffin *et al.* 2009). This process may help to reconcile the LAB thickness based on seismic reflectors (e.g. Rychert *et al.* 2005) with the deeper horizon, seismically imaged as an anisotropic boundary (and also corresponding to the so-called thermal LAB: as T approaches the melting temperature, the material may flow easily and produce seismic anisotropy). The presence of such a chemical boundary within the lithosphere and its complex morphology has been seismically imaged in the North American lithosphere by a high-resolution azimuthal anisotropic model (Yuan & Romanowicz 2010). Several adjustments may be done in future to our compositional structures. In doing this, it will be essential to test their effects on (or invert them from) geodynamic and seismic observations. At this stage, however, it is sufficient for our scopes to model only the first-order ΔC.

Finally, we point out the strong potential of our approach to jointly interpret different seismic data, such as P and S arrival times or SS precursors and long-period waveforms. In principle, our models predict the fine seismic structure of the mineralogical phase transitions and can be therefore used to compute high-frequency seismic phases that are particularly sensitive to mantle discontinuities (such as SS precursors) and compare them with observations. The interpretation of seismic structure corresponding to mineralogical phase transitions is particularly complex, however, and goes beyond our goals. Large ΔV_S are expected in specific depth ranges, particularly between 660 and 800 km, for a realistic thermal structure (Stixrude & Lithgow-Bertelloni 2007). These variations are not imaged by global models, probably because of limited resolution of seismic data. Evidences of strong scattering in the transition zone, especially between 650 km and ∼800 km depth (Kaneshima & Helffrich 2009) could be indicative of the complexities due to phase transformations. More detailed studies are required to understand the effects of mineralogical phase transformations on seismic data. Note that variation in composition is also expected to play an important role, since phase equilibria are modified.

The role of secondary elements that are not included, such as chromium or hydrogen, can be important for modifying the phase

equilibria at a given C (e.g. Klemme 2004; Ohtani & Sakai 2008). The computed phase diagrams with simplified 5- or 6-oxide systems for the principal mantle compositions (i.e. pyrolite) agree well with those determined experimentally, but a precise determination of phase transitions as functions of P, T and C becomes particularly important where these transitions are sharp, for example, at the olivine-wadsleyite boundary (∼410 km). A variation in their modality, for instance, their width and Clapeyron slopes (i.e. $\mathrm{d}P/\mathrm{d}T$), would affect the interpretation of specific seismic phases that are sensitive to sharp impedance ($V_S \times \rho$) jumps, such as *SS* or *PP* precursors (Deuss 2009). In addition, the role of secondary elements on phase equilibria could play an important role on petrological (dynamical) evolution (e.g. Bercovici & Karato 2003) and, consequently, have an indirect effect on seismic interpretation. Previous studies (Deuss 2009; Cammarano *et al.* 2009) showed that, on average, mantle seismic discontinuities are in good agreement with the mineralogical transitions predicted with pyrolite or a similar composition. We recognize, however, that, in the future, an accurate characterization of the phase transitions could shed light on lateral variations in chemical compositions, including water, of the transition zone.

7 CONCLUSIONS

Based on available knowledge of material properties from mineral physics, we interpret a family of recent seismic shear velocity models of the upper mantle for temperature, assuming various compositional structures. In particular, we test the effects of a petrological lithosphere. We found that:

(1) The differences between seismic models translate into quantitatively significant differences in temperature and density, for given composition.
Thermal and density anomalies at a depth of 150 km may vary, respectively, by up to 400 K and 0.06 g cm^{-3} in some locations, which corresponds to ∼70 per cent and ∼80 per cent of the total spatial variations (i.e. min-max value of T and ρ at that depth). These variations considerably exceed those due to uncertainties in modelling the $\partial V_S/\partial T$ of mantle rocks, that are mostly due to anelasticity. Based on extreme anelasticity models, we estimate a maximum variation between −150 and +75 K (less than 20 per cent of total spatial variations) at 150 km depth and below mid-ocean ridges, where the largest effects take place.

(2) Introducing lateral variations in composition does not affect the thermal interpretation much, but it modifies the density structure significantly.
Modelling a petrological lithosphere gives cratonic temperatures at 150 km depth that are only 100 K hotter than those obtained assuming pyrolite, but density is ∼0.1 g cm^{-3} lower. Hence, the density contrasts at lithospheric depths are dominated by compositional variations.

(3) All seismic models show a decrease in velocity from 50 to 100 km below mid-ocean ridges that is in conflict with a simple thermal evolution of oceanic lithosphere. A possible change in the physical mechanism of anelasticity, with water-enhanced effects below a boundary located at ∼65 km depth (Karato 2008), could explain the discrepancy. Further seismic evidence is needed to confirm the decrease with depth of seismic velocity.
The thermochemical models were then analysed for studying relative effects on geoid and topography. We found that:

(4) Structural variations of seismically inferred density models of the transition zone produce significant differences in fitting the geoid, including at degree 2.
We tested density distributions based on different seismic models of the upper mantle, but with same composition, same mineral physics relation for converting V_S into density, same viscosity structure and same boundary conditions. We found that the relative variance reduction between the models is comparable to the relative variance reduction between whole mantle models.

(5) The continental lithosphere is, on average, less depleted (less chemically buoyant) than what is inferred from petrological constraints.
Modelling a petrological lithosphere helps to satisfy both geoid and topography better, but the fit deteriorates if we consider only harmonic degrees $\geqslant$6 for geoid and $\geqslant$12 for topography. Most of the contribution at the longest wavelengths, that helps to improve the fit, comes from the oceanic lithosphere. The signature of the continental lithosphere, instead, induces a worsening of the fit. Including large LVV is not able to eliminate this discrepancy. Therefore, we conclude that the continental lithosphere is, on average, less depleted than what we assume here. This is in agreement with previous findings (Forte & Perry 2000; Perry *et al.* 2003).

An interdisciplinary approach such as the one used here will be essential to produce, in future, better resolved thermochemical models. In general, all our findings indicate that a forward approach is more promising than typical linearized inversion to improve our knowledge of the thermochemical structure of the upper mantle.

ACKNOWLEDGMENTS

We thank two anonymous for comments that improve significantly the manuscript. We thank Takashi Nakagawa for the help given with the geoid computations. This work is partially supported by the European Commission under the Marie Curie Intra-European Fellowship Programme (n. 219870). L.B. thanks Domenico Giardini for his constant support and encouragement.

REFERENCES

Allègre, C. & Turcotte, D., 1986. Implications of a two-component marble-cake mantle, *Nature,* **323**, 123–127.

Artemieva, I.M., 2009. The continental lithosphere: reconciling thermal, seismic, and petrologic data, *Lithos,* **109**, 23–46.

Bassin, C., Laske, G. & Masters, G., 2000. The current limits of resolution for surface wave tomography in North America, *EOS, Trans. Am. Geophys. Un.,* **81**, F897, Fall Meet. Suppl.

Becker, T. & Boschi, L., 2002. A comparison of tomographic and geodynamic mantle models, *Geochem. Geophys. Geosyst.,* **3**, doi:10.1029/2001GC000168.

Bercovici, D. & Karato, S., 2003. Whole-mantle convection and the transition-zone water filter, *Nature,* **425**(6953), 39–44.

Borghini, G., Fumagalli, P. & Rampone, E., 2010. The stability of plagioclase in the upper mantle: subsolidus experiments on fertile and depleted lherzolite, *J. Petrol.,* **51**, 229–254.

Boschi, L., Becker, T. & Steinberger, B., 2007. Mantle plumes: dynamic models and seismic images, *Geochem. Geophys. Geosyst.,* **8**, Q10006, doi:10.1029/2007GC001733.

Boschi, L., Fry, B., Ekström, G. & Giardini, D., 2009. The european upper mantle as seen by surface waves, *Surv. Geophys.,* **30**, 463–501.

Boschi, L., Faccenna, C. & Becker, T., 2010. Mantle structure and dynamic topography in the mediterranean basin, *Geophys. Res. Lett.,* **37**, L20303, doi:10.1029/2010GL04500.

Bozdag, E. & Trampert, J., 2008. On crustal corrections in surface wave tomography, *Geophys. J. Int.,* **172**, 1066–1082.

Cammarano, F. & Romanowicz, B., 2007. Insights into the nature of the transition zone from physically constrained inversion of long-period seismic data, *Proc. Natl. Acad. Sci. USA,* **104**, 9139–9144.

Cammarano, F. & Romanowicz, B., 2008. Radial profiles of seismic attenuation in the upper mantle based on physical models, *Geophys. J. Int.,* **175**, 116–134.

Cammarano, F., Goes, S., Vacher, P. & Giardini, D., 2003. Inferring upper mantle temperatures from seismic velocities, *Phys. Earth planet. Inter.,* **139**, 197–222.

Cammarano, F., Deuss, A., Goes, S. & Giardini, D., 2005a. One-dimensional physical reference models for the upper mantle and transition zone: combining seismic and mineral physics constraints, *J. geophys. Res.,* **110**(B01306), doi:10.1029/2004JB003272.

Cammarano, F., Goes, S., Deuss, A. & Giardini, D., 2005b. Is a pyrolitic adiabatic mantle compatible with seismic data? *Earth planet. Sci. Lett.,* **232**, 227–243.

Cammarano, F., Romanowicz, B., Stixrude, L., Lithgow-Bertelloni, C. & Xu, W., 2009. Inferring the thermochemical structure of the upper mantle from seismic data, *Geophys. J. Int.,* **179**, 1169–1185.

Carannante, S. & Boschi, L., 2005. Databases of surface wave dispersion, *Ann. Geophys.,* **48**, 945–955.

Chapman, D.S., 1986. Thermal gradients in the continental crust, *Geol. Soc. Lond. Spec. Pub.*, **24**, 63–70, doi:10.1144/GSL.SP.1986.024.01.07.

Cobden, L., Goes, S. & Cammarano, F., 2008. Thermo-chemical interpretation of one-dimensional seismic reference models for the upper mantle: evidence for bias due to heterogeneity, *Geophys. J. Int.,* **175**, 627–648.

Cobden, L., Goes, S., Ravenna, M., Styles, E., Cammarano, F. & Connolly, J., 2009. Thermochemical interpretation of 1-D seismic data for the lower mantle: the significance of non-adiabatic thermal gradients and compositional heterogeneity, *J. geophys. Res.,* **114**, B11309, doi:10.1029/2008JB006262.

Connolly, J., 2005. Computation of phase equilibria by linear programming: a tool for geodynamic modeling and an application to subduction zone decarbonation, *Earth planet. Sci. Lett.,* **236**, 524–541.

Deschamps, F., Trampert, J. & Snieder, R., 2002. Anomalies of temperature and iron in the uppermost mantle inferred from gravity data and tomographic models, *Phys. Earth planet. Inter.,* **129**, 245–264.

Deschamps, F., Trampert, J. & Tackley, P.J., 2007. Thermo-chemical structure of the lower mantle: seismological evidence and consequences for geodynamics, in *Superplumes*, pp. 293–320, Springer, Dordrecht.

Deuss, A., 2009. Global observations of mantle discontinuities using ss and pp precursors, *Surv. Geophys.,* **30**, 301–326.

Dziewonski, A. & Anderson, D., 1981. Preliminary reference earth model, *Phys. Earth planet. Inter.,* **25**, 297–356.

Faccenna, C. & Becker, T., 2010. Shaping mobile belts by small-scale convection, *Nature,* **465**, 602–605.

Ferreira, A., Woodhouse, J., Visser, J. & Trampert, J., 2010. On the robustness of global radially anisotropic surface wave tomography, *J. geophys. Res.,* **115**, B04313, doi:10.1029/2009JB006716.

Forte, A., 2007. Constraints on seismic models from other disciplines—implications for mantle dynamics and composition, in *Treatise on Geophysics*, Vol. 1, pp. 805–858, Elsevier, Amsterdam.

Forte, A. & Mitrovica, J., 2001. Deep-mantle high viscosity flow and thermochemical structure inferred from seismic and geodynamic data, *Nature,* **410**, 1049–1056.

Forte, A. & Perry, H., 2000. Geodynamic evidence for a chemically depleted continental tectosphere, *Science,* **290**, 1940–1944.

Forte, A., Quéré, S., Moucha, R., Simmons, N., Grand, S., Mitrovica, J. & Rowley, D., 2010. Joint seismic–geodynamic-mineral physical modelling of african geodynamics: a reconciliation of deep-mantle convection with surface geophysical constraints, *Earth planet. Sci. Lett.,* **295**, 329–341.

Ghosh, A., Becker, T. & Zhong, S.J., 2010. Effects of lateral viscosity variations on the geoid, *Geophys. Res. Lett.,* **37**, doi:10.1029/2009GL040426.

Goes, S. & van der Lee, S., 2002. Thermal structure of the North American uppermost mantle inferred from seismic tomography, *J. geophys. Res.,* **107**, doi:10.1029/2000JB000049.

Grand, S.P., 2002. Mantle shear wave tomography and the fate of subducted slabs, *Phil. Trans. R. Soc. A,* **360**, 2475–2491.

Griffin, W. & Ryan, C., 1995. Trace elements in indicator minerals: area selection and target evaluation in diamond exploration, *J. Geochem. Explor.,* **53**, 311–337.

Griffin, W., O'Reilly, S., Afonso, J. & Begg, A., 2009. The composition and evolution of lithospheric mantle: a re-evaluation and itstectonic implications, *J. Petrol.,* **50**, 1185–1204.

Hammond, W.C. & Humphreys, E.D., 2000. Upper mantle seismic wave attenuation: effects of realistic partial melt distribution, *J. geophys. Res.,* **105**, 10 987–10 999.

Harmon, N., Forsyth, D.W. & Weeraratne, D.S., 2009. Thickening of young pacific lithosphere from high-resolution rayleigh wave tomography: a test of the conductive cooling model, *Earth planet. Sci. Lett.,* **278**, 96–106.

Hill, R., 1952. The elastic behaviour of a crystalline aggregate, *Proc. Phys. Soc. Lond. A,* **65**, 349–355.

Ito, E. & Takahashi, E., 1989. Post-spinel transformations in the system Mg_2SiO_4- Fe_2SiO_4 and some geophysical implications, *J. geophys. Res,* **94**, 10 637–10 646.

Jordan, T., 1981. Global tectonic regionalization for seismological data analysis, *Bull. seism. Soc. Am.,* **71**, 1131–1141.

Kaneshima, S. & Helffrich, G., 2009. Lower mantle scattering profiles and fabric below pacific subduction zones, *Earth planet. Sci. Lett.,* **282**, 234–239.

Karato, S., 1986. Does partial melting reduce the creep strength of the upper mantle? *Nature,* **319**, 309–310.

Karato, S., 1993. Importance of anelasticity in the interpretation of seismic tomography, *Geophys. Res. Lett.,* **20**, 1623–1626.

Karato, S., 2008. *Deformation of Earth Materials: An Introduction to the Rheology of Solid Earth*, Cambridge University Press, Cambridge.

Karato, S., 2010. Rheology of deep upper mantle and its implications for the preservation of the continental roots: a review, *Tectonophysics,* **481**, 82–98.

Karato, S., Jung, H., Katayama, I. & Skemer, P., 2008. Geodynamics significance of seismic anisotropy of the upper mantle: new insights from laboratory studies, *Annu. Rev. Earth planet. Sci.,* **36**, 59–95.

Khan, A., Boschi, L. & Connolly, J., 2009. On mantle chemical and thermal heterogeneities and anisotropy as mapped by inversion of global surface-wave data., *Phys. Earth planet. Inter.,* **180**, 271–282.

Khan, A., Boschi, L. & Connolly, J., 2011. Mapping the Earth's thermochemical and anisotropic structure using global surface wave data, *J. geophys. Res.,* **116**, B01301, doi:10.1029/2010JB007828.

Klemme, S., 2004. The influence of Cr on the garnet–spinel transition in the Earth's mantle: experiments in the system $MgO–Cr_2O_3–SiO_2$ and thermodynamic modelling, *Lithos,* **77**, 639–646.

Kuskov, O.L. & Kronrod, V.A., 2006. Determining the temperature of the earth's continental upper mantle from geochemical and seismic data, *Geochem. Int.,* **44**(3), 232–248.

Kuskov, O.L., Kronrod, V.A. & Annersten, H., 2006. Inferring upper-mantle temperatures from seismic and geochemical constraints: implications for Kaapvaal craton, *Earth planet. Sci. Lett.,* **244**, 133–154.

Kustowski, B., Ekström, G. & Dziewonski, A., 2008. Anisotropic shear-wave velocity structure of the Earth's mantle: a global model, *J. geophys. Res,* **113**(B6), B06306.

Kuvshinov, A. & Olsen, N., 2006. A global model of mantle conductivity derived from 5 years of CHAMP, Oersted, and SAC-C magnetic data, *Geophys. Res. Lett.,* **33**, L18301, doi:10.1029/2006GL027083.

Lekic, V. & Romanowicz, B., 2011. Inferring upper mantle structure by full waveform tomography with the spectral element method, *Geophys. J. Int.*, **185**, 799–831.

Long, M. & Becker, T., 2010. Mantle dynamics and seismic anisotropy, *Earth planet. Sci. Lett.,* **297**, 341–354.

McDonough, W.F. & Sun, S., 1995. The composition of the earth, *Chem. Geol.,* **120**, 223–253.

McKenzie, D., Jackson, J. & Priestley, K., 2005. Thermal structure of oceanic and continental lithosphere, *Earth planet. Sci. Lett.,* **233**, 337–349.

Mitrovica, J. & Forte, A., 2004. A new inference of mantle viscosity based upon joint inversion of convection and glacial isostatic adjustment data, *Earth planet. Sci. Lett.,* **225**, 177–189.

Montelli, R., Nolet, G., Dahlen, F.A. & Masters, G., 2006. A catalogue of deep mantle plumes: new results from finite-frequency tomography, *Geochem. Geophys. Geosyst.,* **7**, Q11007, doi:10.1029/2006GC001248.

Moucha, R., Forte, A., Mitrovica, J. & Daradich, A., 2007. Lateral variations in mantle rheology: implications for convection related surface observables and inferred viscosity models, *Geophys. J. Int.,* **169**, 113–135.

Müller, R.D., Sdrolias, M., Gaina, C. & Roest, W.R., 2008. Age, spreading rates, and spreading asymmetry of the world's ocean crust, *Geochem. Geophys. Geosyst.,* **9**, Q04006, doi:10.1029/2007GC001743.

Ohtani, E. & Sakai, T., 2008. Recent advances in the study of mantle phase transitions, *Phys. Earth planet. Inter.,* **170**, 240–247.

O'Neill, H. & Palme, H., 1998. Composition of the silicate earth: implications for accretion and core formation, in *The Earth's Mantle: Structure, Composition, and Evolution—The Ringwood Volume*, pp. 3–126, Cambridge University Press, Cambridge.

Palme, H. & O'Neill, H., 2003. Cosmochemical estimates of mantle composition, in *Treatise on Geochemistry*, Vol. 2, pp. 1–38, Elsevier-Pergamon Press, Amsterdam.

Panning, M. & Romanowicz, B., 2006. A three dimensional radially anisotropic model of shear velocity in the whole mantle, *Geophys. J. Int.,* **167**, 361–379.

Panning, M., Lekic, V. & Romanowicz, B., 2010. The importance of crustal corrections in the development of a new global model of radial anisotropy, *J. geophys. Res.,* **115**, B12325, doi:10.1029/2010JB007520.

Perry, H., Forte, A. & Eaton, D., 2003. Upper-mantle thermochemical structure below North America from seismic-geodynamic flow models, *Geophys. J. Int.,* **154**, 275–299.

Priestley, K. & McKenzie, D., 2006. The thermal structure of the lithosphere from shear wave velocities, *Earth planet. Sci. Lett.,* **244**, 285–301.

Richards, M. & Hager, B., 1984. Geoid anomalies in a dynamic earth, *J. geophys. Res.,* **89**, 5987–6002.

Ritsema, J., van Heijst, H.J. & Woodhouse, J., 2004. Global transition zone tomography, *J. geophys. Res.*, **109**, doi:10.1029/2003JB002610.

Romanowicz, B., 2009. The thickness of tectonic plates, *Science,* **324**, 474–476.

Romanowicz, B. & Mitchell, B., 2007. Q in the earth from crust to core, in *Treatise on Geophysics*, Vol. 1, pp. 731–774, Elsevier, Amsterdam.

Roux, V.L., Bodinier, J.-L., Tommasi, A., Alard, O., Dautria, J.-M., Vauchez, A. & Riches, A., 2007. The lherz spinel lherzolite: refertilized rather than pristine mantle, *Earth planet. Sci. Lett.,* **259**, 599–612.

Rychert, C., Fischer, K. & Rondenay, S., 2005. A sharp lithosphere– asthenosphere boundary imaged beneath eastern north america, *Nature,* **436**, 542–545.

Simmons, N., Forte, A., Boschi, L. & Grand, S., 2010. Gypsum: a joint tomographic model of mantle density and seismic wave speeds, *J. geophys. Res.,* **115**, B12310, doi:10.1029/2010JB007631.

Stixrude, L. & Lithgow-Bertelloni, C., 2005. Thermodynamics of mantle minerals: I. Physical properties, *Geophys. J. Int.,* **162**(2), 610–632.

Stixrude, L. & Lithgow-Bertelloni, C., 2007. Influence of phase transformations on lateral heterogeneity and dynamics in Earth's mantle, *Earth planet. Sci. Lett.,* **263**, 45–55.

Styles, E., Davies, R. & Goes, S., 2011. Mapping spherical seismic into physical structure: biases from 3-D phase-transition and thermal boundary-layer heterogeneity, *Geophys. J. Int.,* **184**, 1371–1378.

Tackley, P., 2008. Modelling compressible mantle convection with large viscosity contrasts in a three-dimensional spherical shell using the yin-yang grid, *Phys. Earth planet. Inter.,* **171**, 7–18.

Tackley, P., Xie, S., Nakagawa, T. & Hernlund, J., 2005. Numerical and laboratory studies of mantle convection: philosophy, accomplishments, and thermochernical structure and evolution, *Geophys. Monogr. Ser.*, **160**, 83–99.

Tapley, B. et al., 2005. GGM02—an improved earth gravity field model from GRACE, *J. Geod.*, **79,** 467–478, doi:10.1007/s00190-010-0414-2.

Tarantola, A., 2006. Popper, Bayes and the inverse problem, *Nature Phys.,* **2**, 492–494.

Turcotte, D. & Schubert, G., 1982. *Geodynamics*, 2nd edn, Cambridge University Press, Cambridge.

Visser, K., Trampert, J. & Kennett, B., 2008. Global anisotropic phase velocity maps for higher mode Love and global anisotropic phase velocity maps for higher mode Love and Rayleigh waves, *Geophys. J. Int.,* **172**, 1016–1032.

Wenk, H. & Houtte, P.V., 2004. Texture and anisotropy, *Rep. Prog. Phys.,* **67**, 1367–1428.

Xu, W., Lithgow-Bertelloni, C., Stixrude, L. & Ritsema, J., 2008. The effect of bulk composition and temperature on mantle seismic structure, *Earth planet. Sci. Lett.,* **275**, 70–79.

Yang, Y., Forsyth, D.W. & Weeraratne, D.S., 2007. Seismic attenuation near the East Pacific Rise and the origin of the low-velocity zone, *Earth planet. Sci. Lett.,* **258**, 260–268.

Yuan, H. & Romanowicz, B., 2010. Lithospheric layering in the North American craton, *Nature,* **466**(7310), 1063–1068.

Zhang, S. & Christensen, U., 1993. Some effects of lateral viscosity variations on geoid and surface velocities induced by density anomalies in the mantle, *Geophys. J. Int.,* **114**, 531–547.

Zhong, S., McNamara, A., Tan, E., Moresi, L. & Gurnis, M., 2008. A benchmark study on mantle convection in a 3-D spherical shell using CitcomS, *Geochem. Geophys. Geosyst.,* **9**, Q10017, doi:10010.11029/12008GC002048.

SUPPORTING INFORMATION

Additional Supporting Information may be found in the online version of this article:

Supplement. Supporting material includes a section on the effects of lateral viscosity variations (with five figures) and eight supporting figures.

Please note: Wiley-Blackwell are not responsible for the content or functionality of any supporting materials supplied by the authors. Any queries (other than missing material) should be directed to the corresponding author for the article.